



## Calhoun: The NPS Institutional Archive DSpace Repository

---

Theses and Dissertations

1. Thesis and Dissertation Collection, all items

---

1989

### Mapping the airwake of a model DD-963 along specific helicopter flight paths

Anderson, Gustav A.

Monterey, California. Naval Postgraduate School

---

<http://hdl.handle.net/10945/27124>

---

*Downloaded from NPS Archive: Calhoun*



<http://www.nps.edu/library>

Calhoun is the Naval Postgraduate School's public access digital repository for research materials and institutional publications created by the NPS community.

Calhoun is named for Professor of Mathematics Guy K. Calhoun, NPS's first appointed -- and published -- scholarly author.

Dudley Knox Library / Naval Postgraduate School  
411 Dyer Road / 1 University Circle  
Monterey, California USA 93943



DUDLEY HIGH SCHOOL  
DUDLEY, MASSACHUSETTS  
1900





# NAVAL POSTGRADUATE SCHOOL

## Monterey, California



# THESIS

A4536

MAPPING THE AIRWAKE OF A MODEL DD-963 ALONG  
SPECIFIC HELICOPTER FLIGHT PATHS

by

Gustav A. Anderson

December 1989

Thesis Advisor:

J. Val Healey

Approved for public release; distribution unlimited



## REPORT DOCUMENTATION PAGE

1a. REPORT SECURITY CLASSIFICATION Unclassified		1b. RESTRICTIVE MARKINGS	
2a. SECURITY CLASSIFICATION AUTHORITY		3. DISTRIBUTION/AVAILABILITY OF REPORT Approved for public release; distribution is unlimited	
2b. DECLASSIFICATION/DOWNGRADING SCHEDULE		4. PERFORMING ORGANIZATION REPORT NUMBER(S)	
5. MONITORING ORGANIZATION REPORT NUMBER(S)		6a. NAME OF PERFORMING ORGANIZATION Naval Postgraduate School	
6b. OFFICE SYMBOL (if applicable) 67		7a. NAME OF MONITORING ORGANIZATION Naval Postgraduate School	
6c. ADDRESS (City, State, and ZIP Code) Monterey, CA 93943-5000		7b. ADDRESS (City, State, and ZIP Code) Monterey, CA 93943-5000	
8a. NAME OF FUNDING/SPONSORING ORGANIZATION		8b. OFFICE SYMBOL (if applicable)	
9. PROCUREMENT INSTRUMENT IDENTIFICATION NUMBER		10. SOURCE OF FUNDING NUMBERS	
11. ADDRESS (City, State, and ZIP Code)		PROGRAM ELEMENT NO.	PROJECT NO.
12. TITLE (Include Security Classification) MAPPING THE AIRWAKE OF A MODEL DD-963 ALONG SPECIFIC HELICOPTER FLIGHT PATHS		TASK NO	WORK UNIT ACCESSION NO.
13. PERSONAL AUTHOR(S) Gustav A. Anderson		14. DATE OF REPORT (Year, Month, Day) 1989 December	
15. PAGE COUNT 93		16. SUPPLEMENTARY NOTATION The views expressed in this thesis are those of the author and do not reflect the official policy or position of the Department of Defense or the U.S. Government	
17. COSATI CODES		18. SUBJECT TERMS (Continue on reverse if necessary and identify by block number) Turbulence Intensity, Bluff-Body Aerodynamics, Spectrum, Auto-Correlation, Airwake Analysis, Operating Envelopes	
19. ABSTRACT (Continue on reverse if necessary and identify by block number) This study is a continuation from the flow visualization studies done in the NPS low speed environmental wind tunnel. The long term goal is to map the airwake around a ship model and scale to full size for the purpose of determining safe operation envelopes on non-aviation ships. This project utilized hot wire and hot film anemometry to establish a data base for helicopter approach paths of 0°, 30° port, and 30° starboard ship yaw angles. Calibration of the wind tunnel revealed that some turbulence generators, used in the previous two studies, created excessive turbulence intensity levels and were subsequently removed. Analysis along the flight paths was done with and without the model in place. The compari- son showed that turbulence levels of up to 50% were experienced in the proximity of the flight deck. These levels fell by 40 to 50% within $\frac{1}{4}$ ship length along all approach paths. The starboard yaw approach path contained the greatest turbulence magnitudes and the 0° yaw contained the least.			
20. DISTRIBUTION/AVAILABILITY OF ABSTRACT <input checked="" type="checkbox"/> UNCLASSIFIED/UNLIMITED <input type="checkbox"/> SAME AS RPT <input type="checkbox"/> DTIC USERS		21. ABSTRACT SECURITY CLASSIFICATION Unclassified	
22a. NAME OF RESPONSIBLE INDIVIDUAL J. Val Healey		22b. TELEPHONE (Include Area Code) (408) 646-2804	22c. OFFICE SYMBOL Code 67he

1) FORM 1473, 84 MAR

83 APR edition may be used until exhausted.

All other editions are obsolete

SECURITY CLASSIFICATION OF THIS PAGE

\* U.S. Government Printing Office: 1986-806-243

Unclassified

T247827

Approved for public release; distribution is unlimited.

Mapping the Airwake of a Model DD-963  
Along Specific Helicopter  
Flight Paths

by

Gustav A. Anderson  
Lieutenant, United States Navy  
B.S., United States Naval Academy

Submitted in partial fulfillment  
of the requirements for the degree of

MASTER OF SCIENCE IN ENGINEERING SCIENCE

from the

NAVAL POSTGRADUATE SCHOOL  
December 1989

## **ABSTRACT**

This study is a continuation from the flow visualization studies done in the NPS low-speed environmental wind tunnel. The long term goal is to map the airwake around a ship model and scale to full size for the purpose of determining safe operating envelopes on non-aviation ships. This project utilized hot wire and hot film anemometry to establish a data base for helicopter approach paths at 0°, 30° port, and 30° starboard ship yaw angles. Calibration of the wind tunnel revealed that some turbulence generators, used in the previous two studies, created excessive turbulence intensity levels and were subsequently removed. Analysis along the flight paths was done with and without the model in place. The comparison showed that turbulence intensity levels of up to 50% were experienced in the proximity of the flight deck. These levels fell by 40 to 50% within 1/4 ship length along all approach paths. The starboard yaw approach path contained the greatest turbulence magnitudes and the 0° yaw contained the least.

*Thors*  
A 4536  
C.I.

TABLE OF CONTENTS

I.	INTRODUCTION	1
A.	BACKGROUND	1
B.	SHIPBOARD OPERATIONS	9
II.	HOT WIRE ANEMOMETRY	13
III.	EXPERIMENTAL APPARATUS	23
A.	HOT WIRES AND HOT FILMS	23
B.	THE CONSTANT TEMPERATURE ANEMOMETER UNIT AND BRIDGE	25
C.	THE ANALOG TO DIGITAL CONVERTER	26
D.	THE COMPUTER	27
E.	THE TRAVERSE SYSTEM	28
F.	THE DD-963 MODEL	30
G.	THE LOW-SPEED WIND TUNNEL	31
H.	THE "ACQWIRE" SOFTWARE PACKAGE	36
IV.	GENERAL SIMULATION	37
V.	EXPERIMENTAL PROCEDURE	42

VI. DISCUSSION AND RESULTS . . . . .	44
A. CLEAN TUNNEL (NO MODEL PRESENT) . . . . .	44
B. THE ZERO-YAW APPROACH . . . . .	50
C. 30° PORT AND STARBOARD YAW APPROACHES . . . . .	61
D. BRIEF COMPARISON WITH PREVIOUS DD-963 AIRWAKE STUDY . . . . .	80
VII. CONCLUSIONS AND RECOMMENDATIONS . . . . .	81
LIST OF REFERENCES . . . . .	82
INITIAL DISTRIBUTION LIST . . . . .	85

#### **ACKNOWLEDGEMENTS**

My first, and foremost thanks are extended to Professor J. Val Healey for his expert guidance, hands-on assistance, and incomparable patience. For the benefit of their technical and material support, I wish to thank Mr. Al McGuire, Mr. John Moulton, Mr. Ron Ramaker, and Mr. Jack King. For their expertise in computer matters, I would like to thank Mr. Tony Cricelli, Mr. Dave Rigmaiden, and Mr. John Glenn.

## I. INTRODUCTION

### A. BACKGROUND

For surface combatants to meet the requirements of their complex missions, their ability to conduct helicopter operations has become increasingly important. Presently, such ships have the capability to launch, recover, house, and maintain numerous types of helicopters (helos). The role of helos in ships' missions varies from minimal, such as that of most types of cruisers, to primary, as exemplified in FFG-7, DD-963, and FF-1052 class ships. On these ships, helos are a major contributor to the Anti-Submarine (ASW) and Anti-Surface (ASuW) Warfare mission areas.

Safe operating envelopes are determined for each class of ship and its respective helo by the Naval Air Test Center (NATC). This is an expensive and time consuming process, mostly done at sea with each class of ship and the various types of helos the ship is to be certified with. Due to the shrinking number of naval surface combatants, (i.e. FF's, DD's, DDG's) the increased number of operational commitments, and the cost, the process of determining safe operating wind envelopes at sea is no longer feasible. Cheaper, more efficient means must be explored. [Ref. 1: p. 1] In a recent study, Healey [Ref. 2] looked at the feasibility of a

simulation that would encompass models of ship motion, airwake from a ship's superstructure, and helicopter motion. He concluded that good simulation models were under development for ship and helo motion separately however, a good model for the ship airwake and the interface had yet to be developed. A major problem that demands resolution is the ability to quantitatively evaluate the ship airwake and helo interface during launch and recovery. The combined motion of the ship and turbulent airwake generated by a ship's superstructure make launch and recovery the most hazardous phase of ship/helo operations. Presently, shipboard anemometers are used to determine relative wind speeds and direction for the conduction of helo operations.

The current program at the Naval Postgraduate School (NPS) has the overall goal of making detailed airwake maps of model ships and scaling the results to full size with the aim of utilizing these as a data base for simulation. Initially however, the efficiency of single point data modeling will be explored. Single point data involves the acquisition of data at single points in a flowfield and analyzing various statistical information (i.e. mean, standard deviation, autocorrelation, etc.) to determine velocity components, turbulence intensities, and energies present in the turbulence, for mathematically modelling the airflow. The flowfield around DD-963 Spruance Class destroyer has

previously been studied using flow visualization techniques and it was concluded that air flow over the model ship was (1) a very strong function of the ship's yaw angle, (2) vortical in nature, and (3) extremely turbulent with strong recirculating currents. [Ref. 1: p. 42] The present study is an essential prerequisite to the current program which involves quantitative analysis of the ship airwake using hot wire and hot film anemometry. This project will look at wind velocities and other statistical properties of the airwake of a model DD-963 (1/141 scale) in a simulated atmospheric boundary layer using 3-D hot wire anemometry at various positions relative to the ship model along typical helo approach flight paths. In practice, the approach paths vary with true and relative wind direction, helo and ship velocity, loading of the helo, and sea state. It is the hope that, if this simulation is successful, the methods developed in the present study may be extended to other ship models for evaluation of their respective ship airwakes.

In 1976, T. S. Garnett of the Boeing Vertol Company, conducted wind tunnel tests examining the ship generated airwake of a model (1/50 scale) FF-1052 Class Frigate. The results were used in formulating math models of airwake turbulence created by the ship and its superstructure. [Ref. 3: p. 9] R.L. Fortenbaugh, of the Vought Corporation, developed mathematical models for DD-963 ship motion and

airwake in an effort to look at the feasibility of DD-963 Class Destroyers operating with Vertical, Short Take-off and Landing (VSTOL) aircraft. Completed in 1978, the simulation resulting from this effort will be discussed later. In developing the airwake model, the Boeing Vertol FF-1052 airwake data base was used and Strouhal scaled by Fortenbaugh to the DD-963 geometric specifications, a process that has no scientific basis; however, Fortenbaugh recommended that the data base be replaced by DD-963 data once available. [Ref. 4: p. 9] In 1980, Garnett conducted wind tunnel tests with a 1/80 scale DD-963 model. Presently a modified version of Garnett's data is used as a data base in DD-963 airwake modeling. [Ref. 5: p. 113]

Of note in the two Boeing projects is the fact that the data were taken under the conditions of a constant velocity profile and almost zero turbulence. The ship models were mounted on a ground plane elevated off the floor to lift it out of the wind tunnel boundary layer and expose it solely to the uniform flow. In effect, this process reproduced ship generated winds. On the other hand, in neutral winds, the earth's atmosphere is a sheared turbulent boundary layer and proper simulation of its velocity and turbulence profiles must be considered when conducting wind tunnel tests. Winds which have blown over a fully developed rough sea are turbulent and are characterized by: (1) windspeed averaged over some time

period or temporal speed average, (2) turbulence intensity (the standard deviation of the along-wind windspeed divided by the mean windspeed), (3) the longitudinal scale length of the turbulence (the mean length of the most energetic eddies in the turbulence), and (4) the spectrum function of the turbulence, which indicates how the energy is distributed amongst the frequencies present in the turbulence. [Ref. 2: p. 4] In addition, the ship airwake is a function of the above plus the wind/ship speed ratio (due to the effects on turbulence intensity) and the relative wind direction which is a function of ship's yaw angle.

Empirical relationships are available from the Engineering Sciences Data Unit (E.S.D.U.) [Ref. 6] which show that the free stream flow parameters are functions of the mean windspeed, elevation from the surface or mean wave height, and the roughness length scale of the sea. According to Davenport, [Ref. 7: p. 548] over rough seas, the surface roughness length scale is usually between 0.001 and 0.01 meters. Elevation is taken as flight deck height above the mean wave height or the position of the helo during launch and recovery. Windspeed and elevation are related in the equation  $U/U_{ref} = (Z/Z_{ref})^n$  where  $U$  is the along-wind velocity at a specific elevation,  $Z$ .  $U_{ref}$  and  $Z_{ref}$  are the free stream velocity and height respectively at some reference point. [Ref. 8: p.579] The factor "n" is a constant and should be

matched in the wind tunnel and full scale flows. For tunnel calibration, the "Z" will be the height at the top of the boundary layer (about 0.8m) and the  $U_{ref}$  will be the velocity at that height. For data acquisition in the airwake, it is more appropriate to reference the measurements to the velocity at ship anemometer elevation.

Exact duplication of every aspect of the atmospheric flow field at a smaller scale is impossible; however, simplifications are permitted due to the special nature of the atmospheric boundary layer. Modelling of the wind profile is generally possible for a neutrally stratified boundary layer; an exception is the intermittency in the flow. A low speed wind tunnel at NPS has had a thick boundary layer set up using the procedures established by Counihan [Ref. 8: p. 590] with upstream vortex generators and additional turbulence generators to provide a simulated atmospheric boundary layer. Velocity profiles for the Boeing Vertol tests and the NPS tunnel are shown below in Figure 1.

An element of this project is to compare the NPS and Boeing Vertol DD-963 data. It is noteworthy that the Boeing study used up to ten 3-D split film hot wire probes in their tests and used a large, crude, and non-streamlined mechanical support device that almost certainly generated flow interference. In the NPS tunnel, the probe will extend well forward of its supports to eliminate, or at least minimize,

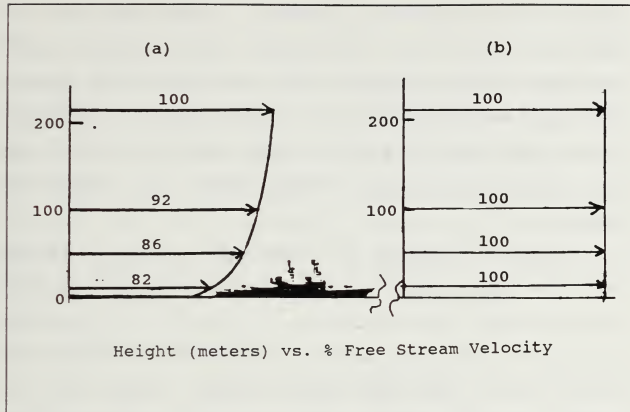


Figure 1. Velocity Profiles for (a) NPS Wind Tunnel and (b) Boeing Vertol Tests

possible interference. Boeing Vertol indicated that they found no spatial correlation between their probe signals; however, no attempt was made to rigorously analyze the test data for math modelling purposes. Single point data will be obtained in the NPS tunnel and autocorrelations will be used to estimate the length scales in the flow. If the turbulent velocity fluctuations are small compared with the mean along-wind velocity, the eddies of the turbulence should not change appreciably in shape and, with autocorrelation, eddy sizes can be estimated [Ref. 9: p. 30]. These single point data will

be used in an attempt to obtain a simple data base for validation of the existing simulator models. If the single point data proves unsuccessful, the NPS model will be expanded to include multiple data points to obtain spatial correlations between the various hot wire probes. Such data will be used in conjunction with more sophisticated helo mathematical models.

A ship is an example of a bluff body - one with a massive separated wake. A most important feature of such sharp-edged bodies is that there is essentially no change in flow patterns when the flow Reynolds number is above a certain low minimum. With a constant beam based Reynolds number greater than about 10,000, viscous to inertial simulation of the ship airwake can be achieved using wind tunnel speeds of 1.2 m/s and above. However, if the wake of an oscillating ship is to be modeled, due to the frequency limitation on the oscillating mechanism, the ship's airwake can be modeled in a tunnel with equality of Strouhal number (frequency of ship's oscillation \* ship's beam / free stream velocity), only if the velocity is approximately 3 m/s or less. In the present study, this Strouhal number equality is unnecessary because the model is stationary. However, it will be used to determine the frequency ratio between the turbulence around the scaled model and that on the full sized ship. Assuming the wind gust frequency necessary to move a helo, as a whole, of at most 1

Hz in a wind of 20 m/s (about 40 knots) and a tunnel boundary layer effective wind velocity of 2 m/s at about helo-deck height, measurements will need to take turbulence frequencies below 14.1 Hz into account. Since this goal is easily met, the filter cut-off frequency will be set at much higher levels so that the data can be used for vehicles much smaller than helos. This will be discussed further at a later point. Future studies incorporating ship motion will have to take Strouhal scaling of the ship motion into account.

#### **B. SHIPBOARD OPERATIONS**

The DD-963 "Spruance-Class" destroyer is one of the surface navy's primary players in ASW, ASUW, and carrier escort operations. This multi-mission ship's ability to conduct operations is greatly enhanced by its ability to launch and recover helos. The ship is 563 feet long with a beam of 55 feet. Displacement ranges between 7200 and 7800 tons. Numerous types of helos are certified to conduct operations with the DD-963 including the SH-2F, SH-3, CH-46, and the SH-60. Most of the 963s embark an SH-2F detachment for work-ups and deployment. Some 963s have been retrofitted with the Recovery Assist, Secure and Traverse System (RAST) for use exclusively for the SH-60 helicopter.

The flight deck is located aft of the helo hangar on the 02 level 33 feet above the waterline with a 2200 square foot

landing pad. Between the landing area and the hangar on the same deck is 440 square foot area used for the helo refueling hose reel, the Twin Agent System for firefighting, and space to provide room for the landing signalman during helo evolutions. (See Figure 2) The hangar is 49 feet long, 26 feet wide and 18 feet high. On top of the helo hanger, on the starboard side, are the exhaust stacks for the number two engine room's two propulsion gas turbines and its gas turbine electric generator. These stacks protrude from a 20 X 14 X 10 foot pedestal. Also on top of the hangar are the Mk 15 Close In Weapons System and its magazine, small pyrotechnic lockers and the Stabilized Glide Slope Indicator (SGSI).

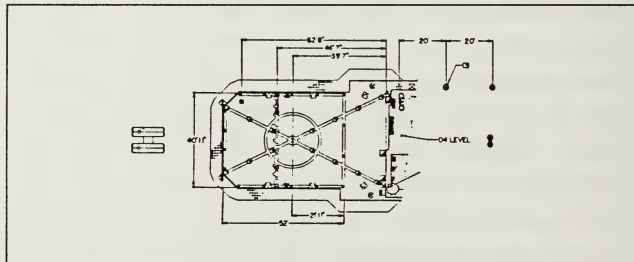


Figure 2. DD-963 Flight Deck Diagram [Ref. 10]

The 963 also has two vertical replenishment (VERTREP) stations, one on the forecastle and one on the fantail (01 and main deck levels respectively). These stations are used primarily for 5"/54 ammunition on-loads with VERTREP from CH-46 helo with underslung loads.

Prior to conducting a launch or recovery, the ship is brought to a course and speed to which the relative wind is within the wind operation envelope for the evolution being conducted. Operating envelopes such as Figures 3 and 4 are published in Naval Warfare Publication (NWP)-42(Series). They also include maximum pitch and roll permissible for the ship to conduct launch and recover evolutions. Numerous envelopes are available based on day or night operations, starboard or port approaches, and rotor engagements and disengagements. A discussion with some pilots at NPS revealed that most prefer relative winds 20-30 degrees of either port or starboard bow at 15-25 knots, however, preferences can change with different pilots. This operating condition is well within most helo and ship operating envelopes. The present project will concentrate 30° starboard, port, and stern approach paths out to one ship length aft of the touchdown point.

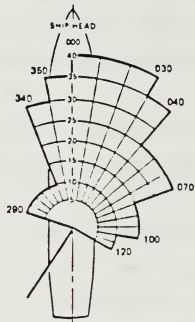


Figure 3. Typical DD-963  
Operating Envelope - Day  
Starboard Approach. [Ref. 11]

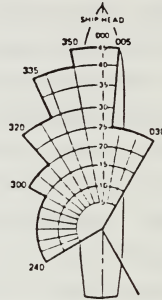


Figure 4. Typical DD-963  
Operating Envelope - Night  
Port Approach [Ref. 11]

## II. HOT WIRE ANEMOMETRY

Hot wire anemometry involves the use of a thermal anemometer to measure the velocity and its fluctuations in a fluid flow. This is accomplished by placing a "hot wire," essentially a very small diameter heated sensor spanning support prongs, as one leg of a Wheatstone bridge, and measuring the voltage change as the fluid flows by. The sensor thus cools, due to convective heat loss, causing its resistance and the voltage across the prongs to fluctuate with the varying speeds. To maintain the sensor at constant temperature, the current is rapidly varied by a control circuit to almost instantaneously balance the bridge network and correct for the heat loss from the sensor. Voltage variations (due to the changing current) are measured and from this, velocity information can be determined.

In addition to the convective heat transfer from the wire to the passing fluid, other factors that contribute to the heat loss are operating temperature, geometry, thermal conductivity of the sensor, characteristics of the passing fluid, and radiation and end conduction losses. The sensor, usually at a minimum temperature above 200°C will naturally transfer heat to the cooler flowing (or still) air around it. The bridge circuitry provides the voltage that attempts to

maintain the sensor at constant temperature. The sensor is usually small and presents minimum thermal inertia. Hot wire sensor diameters are usually between 5 and 9 microns, with lengths of about 2 to 3 millimeters (mm). In both 3-D films and wires, the active length of the sensor is only about 1.25 mm. This is to minimize interference and end conduction losses. Hot film sensors are about 70 microns in diameter. The sensor must have a high temperature coefficient of resistance (TCR), a constant which relates resistance change with temperature. This permits interpretation of voltage fluctuations in terms of velocity fluctuations. Three dimensional tungsten wire sensors and nickel film probes are used in this project with coefficients of 0.42% and about 0.45% respectively [Ref. 12: p. 9]. The passing airflow in the wind tunnel is sufficiently low in speed to be considered incompressible and isothermal. End conduction losses occur, even though the supporting legs are much thicker than the sensor and are not heated appreciably by the flowing current; this loss must be accounted for and calibration under operating conditions ensures this. Radiation losses are negligible being less than 0.1% of the convection loss. With these assumptions, heat loss by the sensor can be considered a direct measure of the passing fluid velocity. [Ref. 13: p. 101]

Sensor temperature is usually expressed as a ratio called the "overheating" or "overheat ratio." This relates hot resistance to ambient resistance. Wires and films are given a sufficiently high value of overheating to obtain optimum sensitivity, a high signal-to-noise ratio for the electrical circuit, and a large output signal. [Ref 12: p. 6] An important part of the processes of calibration and data acquisition is determining the operating resistance of the system. The total operating resistance of the probe,  $R$  can be expressed by the equation:

$$R = R_{\text{total}} + \alpha R_{\text{Ambient}} [T_{\text{Hot sensor}} - T_{\text{Ambient}}]$$

where  $R_{\text{Total}} = R_{\text{Lead+Sensor+Cable}}$ ,  $T$  = Temperatures,  $\alpha$  = TCR, and  $R_{\text{Ambient}}$  = Resistance of the sensor at ambient temperature [Ref. 12: p. 9]. Heating the sensor increases its resistance and cooling due to the passing fluid decreases it. The reduced resistance lowers the voltage across the bridge which in turn lowers its input to a control amplifier. This amplifier fluctuates its output inversely proportional to the resistance change in the sensor. Hence more current is fed back to restore the wire or film to its initial temperature and resistance and balance the circuit. [Ref. 14: p. 2] Proper amplifier gain setting is important to ensure immediate and proper response of the bridge. The DANTEC 56C17 Constant Temperature Anemometer Bridge and the 56C01 CTA unit are used in this project to make up the flow anemometer.

Calibration of the constant temperature anemometer is done basically by recording output voltages over 10 to 15 known velocities and creating a calibration curve. A problem in determining the turbulence levels in a real flow is the non-linearity in the relationship between voltage and velocity. These are caused by (1) the non-linear nature of the heat transfer and, (2) quadratic non-linearities due to transverse velocity perturbations [Ref. 15: p. 118]. Electronically linearizing an analytically generated function about some appropriate mean is the best way to circumvent the problem. As long as turbulence intensities are relatively small, small perturbations in the mean velocity may be quantitatively determined [Ref. 16: p. 275]. It is a matter of opinion how small "relatively small" is; the pessimists give up to 8-10% and the optimists up to 25-30%. The Dantec 56N21 Electronic Linearizer can be placed in the path between the CTA unit and the Analog to Digital (A/D) converter. Its transfer function is automatically adjusted to be the inverse of the anemometer's transfer function, hence cancelling velocity information distortions. [Ref. 17: p. 2] Unfortunately, electronic linearizers were not available for all channels at the time of the present project and were not used.

After the sensor is installed and the CTA Bridge is set to the proper overheating ratio, the calibration can be accomplished with the use of King's Law for convective

cooling:  $E^2 = A + BU^n$ , where  $E$  is the voltage output,  $A$  and  $B$  are dimensional constants, and  $U$  is the effective velocity. For velocities between 0.3 and 80 m/s,  $n$  is generally accepted to be 0.45. Another way to develop a calibration curve is through the use of a software program that generates calibration polynomials for each wire or film. The polynomial is of the form:

$$U = C_1 + C_2E + C_3E^2 + C_4E^3 + \dots$$

where  $C_n$  are calibration coefficients of the polynomial to be determined in the calibration process, and  $E$  is the voltage output from the bridge. The program computes the coefficients of this polynomial of the prescribed degree for each wire of the 3-D probe. The program has the capability to output the calibration points with the curve generated by the polynomial and an error plot for each wire. For the calibrations in this project, the polynomials have had an error of less than 4%. To accomplish the calibration, the Dantec 55D90 Calibration Equipment is used to produce known velocities. It generates a variable velocity, low-turbulence (< 5%) free air jet. The 5% design turbulence is found at the low end velocities (1-4 m/s) that will be encountered in this project. This is desirable, since this turbulence represents conditions closer to the operating conditions than to a smooth jet flow. A block diagram of the 55D90 is shown in Figure 5 and a pictures of the 55D44 (Pressure Control Unit), 55D45 (Nozzle Unit with

variable area nozzles), and 55D46 (Pressure Converter) are shown in Figure 6.

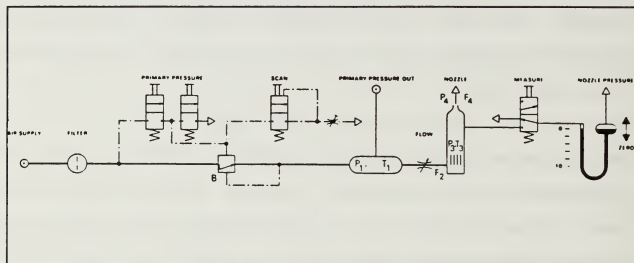


Figure 5. Diagram of 55D90 Calibration Equipment  
[Ref. 18: p. 3]

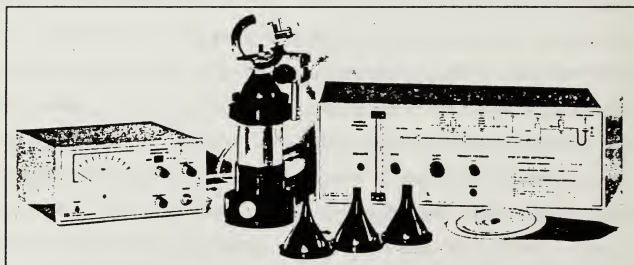


Figure 6. Pressure Control Unit with Pressure Converter,  
Nozzle Unit with Variable Area Nozzles [Ref. 18: p. 2]

Primary pressure (the set pressure in the primary chamber of the 55D90) is read by the pressure converter and its electrical output is read by a Compaq 386/25 computer through the Analog-to-Digital (A/D) converter. A scan feature is used to produce a steadily decreasing velocity from the output nozzle. The pressure converter is a linear function of the velocity to within 1%, and its readings are initially placed in a file together with the voltage readings from the three wires (or films). [Ref. 18: p. 4] The acquisition program accepts the four readings; three voltages and one pressure.

Table I(a) shows an example of a calibration file. Channels 0, 1, and 2 contain the voltages for the three wires and channel 3 holds the value for primary pressure corresponding to the voltage readings at that point. The first column in the file is assigned for velocities and is not affected in this acquisition process. The pressures are then manually converted to velocities and overwritten into the first column of the file. Once this is done, the pressure readings can be eliminated and the table of the remaining three voltages and corresponding velocities exists as shown in Table I(b). The voltages are then processed to produce calibration polynomials for each wire. The polynomials are then used in the data acquisition and processing phase to determine the airwake velocities from the raw voltages.

The computed velocities are then further processed to moments, autocorrelations, and spectrum functions.

Table I. (a) Acquisition Calibration File  
 (b) Velocity Converted Calibration File with Pressures  
 Eliminated

Point	u	chan 0	chan 1	chan 2	chan 3
(a)	1	2.2481	2.2885	2.2557	9.0340
	2	2.2242	2.2634	2.2315	8.3940
	3	2.1622	2.1886	2.1564	6.5742
	4	2.1123	2.1444	2.1137	5.6829
	5	2.0749	2.1010	2.0711	4.8570
	6	2.0402	2.0646	2.0432	4.2139
	7	2.0095	2.0390	2.0021	3.6803
	8	1.9793	1.9982	1.9780	3.2127
	9	1.9525	1.9765	1.9408	2.8208
	10	1.9264	1.9404	1.9124	2.4882
	11	1.8991	1.9113	1.8841	2.1583
	12	1.8755	1.8857	1.8581	1.8830
Point	u (m/s)	E <sub>x</sub>	E <sub>y</sub>	E <sub>z</sub>	(all volts)
(b)	1	4.00	2.2481	2.2885	2.2557
	2	3.72	2.2242	2.2634	2.2315
	3	2.91	2.1622	2.1886	2.1564
	4	2.52	2.1123	2.1444	2.1137
	5	2.15	2.0749	2.1010	2.0711
	6	1.87	2.0402	2.0646	2.0432
	7	1.63	2.0095	2.0390	2.0021
	8	1.42	1.9793	1.9982	1.9780
	9	1.25	1.9525	1.9765	1.9408
	10	1.10	1.9264	1.9404	1.9124
	11	0.96	1.8991	1.9113	1.8841
	12	0.83	1.8755	1.8857	1.8581

To ensure that the coordinate system of the hot wire is in concurrence with that of the wind tunnel, a check can be accomplished using the nozzle unit and the 3-D probe. The nozzle unit has a probe support mechanism that allows the probe to be pitched or yawed to within + or - 1/2 a degree.

By design, the Dantec software contains a default coordinate correction matrix which transforms the coordinate of the probe to that of the wind tunnel, providing that the number-3 wire is in the vertical plane. Once calibration polynomials are generated, proper orientation of the probe can be checked by adjusting the pitch and yaw to arbitrary angles on the nozzle unit. To acquire data, a separate module of the software is entered which applies Jorgensen coefficients (the default coordinate correction factors) and calculates the three velocity components (U,V, and W). [Ref. 19: p. A-2] The angles of pitch and yaw can be determined readily by using simple trigonometry. The directional accuracy of the data acquisition/processing can then be determined by placing the probe in the calibrator at specific pitch/yaw angles and comparing these angles with those calculated; such tests have shown that this method is accurate to within 3°. Alignment of the probe in the wind tunnel is accomplished by using a leveled transit and sighting the number-3 wire in the vertical plane.

The primary differences between hot films and hot wires lies in their construction, noise levels and high frequency response. In the hot-film fabrication process, a 0.5 micron thick film is mounted on a non-electrically conducting quartz substrate which acts as a thermal insulator and provides rigidity to the thin film. The latter is made of nickel and

is placed onto the quartz by vacuum sputtering - a process by which uniform thickness of the sensing element is obtained. Hot films are more durable but have a lower frequency response above about 10,000 KHz. There are also heat conduction losses through the substrate and the film's maximum operating temperature is slightly higher than that of hot wires. The films also have a higher temperature coefficient of resistance and much higher electronic noise levels at about 1 KHz. The significant frequencies encountered in the present project were below 100 Hz and the difference in noise levels between the wires and films is not very important. Furthermore, the poorer frequency response of the film is unimportant for the same reason. This study was initiated using hot-wires and then switched to hot-films, when the more delicate wires incurred damage. The calibration process of the film is the same as that for the wires.

### III. EXPERIMENTAL APPARATUS

The equipment and software used in this project were:

- A. Dantec 55R91 and 55P91 Hot Wire and Hot Film Probes.
- B. Dantec 55C01 CTA Unit and 56C17 Bridge.
- C. MetroByte DASH-16 Analog to Digital Converter.
- D. Compaq 386/25 Micro Computer.
- E. Tri Sigma Corp. 8352 Traverse Controller.
- F. DD-963 Model.
- G. Low Speed Environmental Wind Tunnel.
- H. Dantec "acqWIRE" Software Package.

#### A. HOT WIRES AND HOT FILMS

Table II represents the parameters of the hot wire and hot film sensors used in this project [Ref. 12: p. 9]. The 3-D hot wire and film probes used were the Dantec 55P91 and the 55R91 respectively. Each probe has three mutually perpendicular sensors mounted so that the horizontal direction of the flow is inside a cone of 70.4 degrees (35.2 degrees in any direction from the x axis). This configuration is preferred to avoid support prong interference and thermal crosstalk between the sensor wires due to their hot wakes. [Ref. 12: p. 4] A probe mounted in the 55D45 Nozzle Unit is shown in Figure 7.

Table II. Hot Wire and Hot Film Parameters

	HOT WIRE	HOT FILM
Material	Tungsten	Nickel
Diameter	8.89 microns	70 micron 0.5 micron thickness
Active Length	1.25 mm	1.25 mm
Ambient (20 C)	0.6 Ohms	4.30 Ohms (Film 1)
Temperature (All wires)		4.26 Ohms (Film 2)
Resistance		4.35 Ohms (Film 3)
Temp. Coef. of Resist.	0.42%	0.45%
Max Temp.	300 C	300 C
Min Vel.	0.2 m/s	0.2 m/s
Frequency	300 kHz	175 kHz

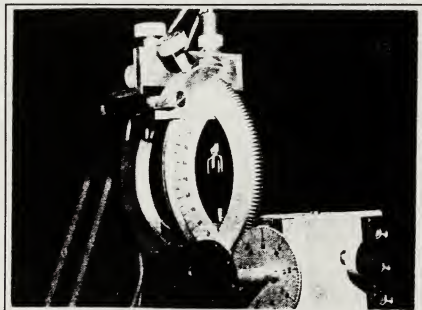


Figure 7. 3-D Probe Mounted in  
55D45 Nozzle Unit

## B. THE CONSTANT TEMPERATURE ANEMOMETER UNIT AND BRIDGE

The Dantec 56C01 Constant Temperature Anemometer together with the 56C17 CTA Bridge constitute a complete constant temperature anemometer, producing an analog signal. The complete unit is shown in Figure 8. The leads of the 3-D probe are connected via 20 meter coaxial cables to the 56C17 Bridge to form one arm of the Wheatstone bridge. A feedback circuit provides for a voltage over the adjusted bridge resistance even with the probe in a stationary atmosphere, since there will be heat loss even then from the sensor due mostly to natural convection [Ref. 14: p. 2].

The operating temperature is determined by the fixed, nominal overheat ratio defined as:  $a = (R - R_o) / R_o$  where  $R_o$  is the ambient temperature resistance of the wire (or film) and  $R$  is the heated sensor resistance [Ref. 14: p. 8]. BCD switches on the front of the 56C17, together with the 56N22 Mean Value Unit acting as a digital voltage display, allow the operator to measure the probe/lead/cable combination resistance and to adjust for the desired overheat. Internal switches in the bridge allow the operator to make adjustments for different cable lengths, gain and upper frequency limit settings, and for the type of sensor (film or wire). Optimum settings for gain and upper frequency limit need to be determined during the data acquisition trials. The CTA unit

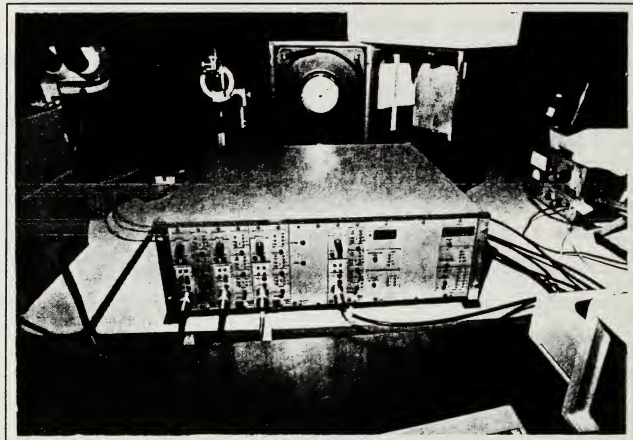


Figure 8. 56C01 and 56C17 CTA Unit

has a built-in square-wave generator which allows the frequency response to be optimized.

#### C. THE ANALOG TO DIGITAL CONVERTER

Analog to digital (A/D) conversions are made through the MetraByte Corporation 12 bit Dash-16 successive approximation converter. With a 10 volt range, it is accurate to 2.44 millivolts. Digital representation of the time dimension is done implicitly, where analog to digital conversion are successively triggered by a clock, at a sampling frequency of

1000 Hz (for this project) and stored into direct memory access [Ref. 20: p. 3-8]. The sampling rate can be varied and must be greater than the rate at which significant changes in the analog signal's amplitude can occur. In the frequency domain, the sampling rate must be at least twice the highest frequency that is expected to be encountered; otherwise readings will be in error due to aliasing. [Ref. 20: p. 3-29] With the 1000 Hz sampling rate, the latter will be avoided in the present study; this figure was obtained from preliminary data analysis which showed insignificant energy levels in the spectrum above a few hundred Hz. The A/D board has a 12 micro second conversion time with a software controlled trigger. It also has a low-drift, fast settling instrumentation amplifier/sample-hold combination to ensure that the signals from all three channels of the hot wire (or hot film) probe are read virtually simultaneously. [Ref. 21: p. 3]

#### D. THE COMPUTER

The Compaq 386/25 micro computer, shown in Figure 9 (along with the HP 7475A Graphics Plotter) is a 25 MHz machine with an 80386 main central processing unit. There are two math coprocessors, the 80387 and the Weitek 6117 chip used for addition/subtraction/series operations. The computer has a 300 M-byte hard disk with a 1.2 M-byte 5-1/4" and a 1.44 M-byte 3-1/2" floppy capability. In addition, there is a 16 M-



Figure 9. Compaq 386/25 Micro Computer  
with HP 7475A Graphics Plotter

byte random access memory and video graphics arrays with 800 X 600 pixels. Finally, it also has a 80235 cache controller and the Compaq MicroSoft-DOS version 3.31 is implemented.

#### E. THE TRAVERSE SYSTEM

The position of the probe in the tunnel is controlled by the Tri Sigma Corporation 8352 Controller. (Figure 10) The probe is mounted on an arm, as pictured in Figure 11, and positioned well forward toward the direction of the flow and



Figure 10. Tri Sigma 8352 Traverse Position Controller

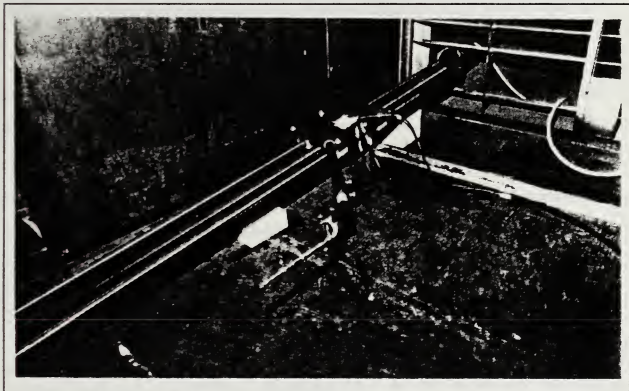


Figure 11. Traverse Slide with Probe on Mounting Arm

away from the supporting structure. The 8352 is capable of measuring precise position relative to the flight deck of the model. The system is accurate to within 1/12 mm. per meter. (0.001 inch per foot). [Ref. 22: p. 67] The traverse slide manufactured by Linear Industries, is 1.8 meters (6 ft) long, and is mounted in the tunnel at an angle of 4 degrees to simulate the approach path of a helo. The slide is supported from below by two wooden blocks cut at the 4 degree angle. A ramp is placed in front of the leading edge to divert flow as smoothly as possible past the slide. The angle of inclination can be varied by simply replacing the wooden blocks with blocks cut at different angles.

#### **F. THE DD-963 MODEL**

The model DD-963 (Figure 12) used in the project was constructed of wood by a private modelmaker in the Philippines. It was fabricated from the blueprints provided by the Supervisor of Shipbuilding, Conversion and Repair in Pascagoula, Mississippi which were reduced to a suitable scale at NPS. These unclassified blueprints were of hull curves of form, port and starboard profile, and bow, stern, and top aspects. This is the same model as used in the NPS project of the DD-963 airwake flow visualization. [Ref. 1: p. 16] It is 1.22 meters long (1/141 scale) and is mounted on a mechanism designed to dynamically simulate pitch, roll, and

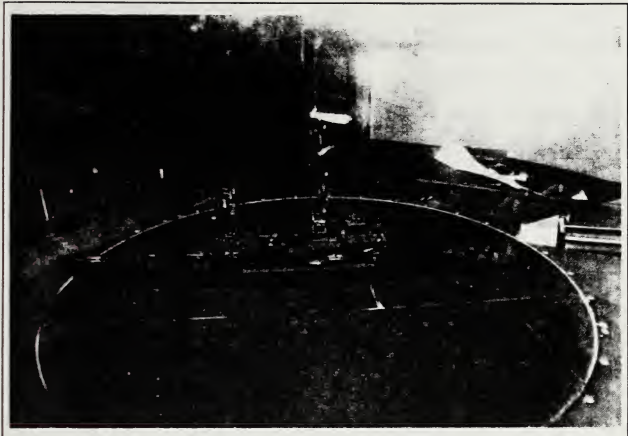


Figure 12. DD-963 Model

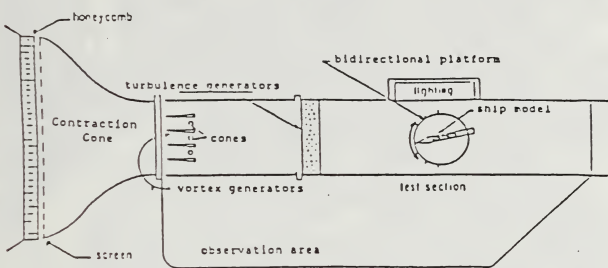
heave. The mechanism can be adjusted to provide various static angles of roll, pitch, and yaw. The floor has a circular insert around the model to provide for these yaw adjustments. To prevent the flow of air in or out of the tunnel during operation, foam weather stripping is attached (glued) to the circular floor piece around the model.

#### G. THE LOW-SPEED WIND TUNNEL

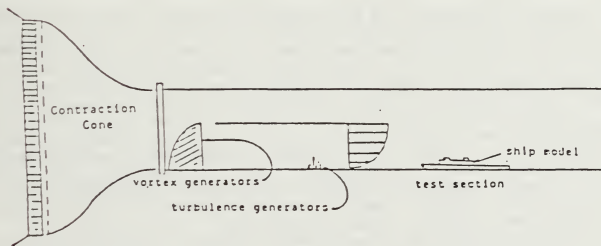
The open circuit, low-speed, flow-visualization wind tunnel has been modified to simulate the atmospheric boundary layer over a rough sea. The tunnel is powered by a 25 Horse

Power electric motor driving a fan capable of generating test-section free-stream velocities of up to 9.6 m/s (31.5 ft/s). Air enters through a 20.9 m<sup>2</sup> (225 ft<sup>2</sup>) section and passes through a 76 mm (3 inch) long honeycomb and mesh diffuser. With a 9-to-1 square bell contraction cone, air proceeds to the 2.32 m<sup>2</sup> (25 ft<sup>2</sup>) test section. The test section is square with dimensions of 1.52 X 1.52 m (5 X 5 ft). This section is 6.7 m (22 ft) long and at its exit, air passes through the fan and exhausts to the atmosphere.

Figure 13 shows top and side views of the tunnel [Ref. 22: p. 19]. At the beginning of the test section of the tunnel are four vortex generators as mentioned in the introduction. They are 0.79 m (31 inches) tall and are constructed of aluminum angle pieces, which provides strength and rigidity, and styrofoam filling. A boundary layer of about the same height as the vortex generators is created as air flows by. It is felt that the major superstructural elements of any model used in the overall project will be less than about 20% of that height. This is to ensure that the model is within the so-called surface layer of the boundary layer. A full scale ship at sea would never exceed 20% of the height of the atmospheric boundary layer in a rough sea. [Ref. 7: p. 549] The full scale size of this simulated boundary layer would be over 100 m (325 ft). The upper mast of the DD-963 model stands a maximum of 0.28 m (11 inches)



Plan View



Elevation

Figure 13. Top and Side Views of Tunnel Layout [Ref. 23]

from the floor with the flight deck at 76 mm (3 inches).

The vortex generators produce the shear and some of the turbulence in the tunnel. They are quarter elliptical in shape when viewed from the side and triangular (or wedge shaped) when viewed from the top or in any horizontal section. They have a sharp leading (windward) edge and widen to a maximum of 76 mm (3 inches) in width at the base. To further refine the velocity profile, three 0.76 m (30 inch) high, 51 mm (2 inch) diameter tapered cones were added and placed equidistant between the vortex generators. The cones and the vortex generators were all connected at the top with a 1.52 m (5 ft) long, aluminum support rod of airfoil shape and with the chord parallel to the flow. Further downstream, more turbulence was generated by roughness elements, or turbulence generators as shown in Figure 14. Also shown in Figure 14 (looking upstream) are the vortex generators and at the bottom of the photo the model is shown. 9.5 mm (3/8 inch) diameter wooden dowels of varying lengths between 25 and 152 mm (1 and 6 inches) were placed on a 0.46 X 1.52 m (1.5 X 5 ft) peg board on the floor of the tunnel. These dowels were necessary to bring turbulence intensity levels to a realistic value at flight deck height. [Ref. 1: p. 13]

At the time this boundary layer was established by Bolinger, [Ref. 23] no accurate means were available to measure velocities below about 1.5 m/s, since this corresponds

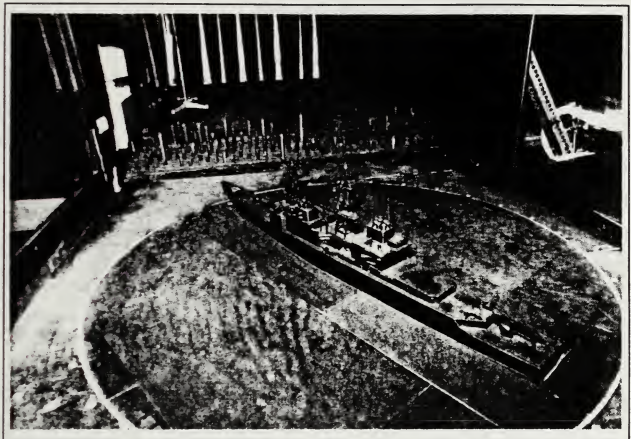


Figure 14. View Upwind of Model, Turbulence Generators and Vortex Generators

to about 1/4 mm (0.01") of water height; the result was that, at the lowest two points in the layer, the velocities obtained were somewhat higher and turbulence levels measured lower than they actually were. It was found that the additional turbulence generators could be removed, which allowed the velocity to increase near the floor, without causing the turbulence levels to drop below those previously reported in References 1 and 23.

## H. THE "ACQWIRE" SOFTWARE PACKAGE

The Dantec "Acqwile" software package was installed into the Compaq 386/25 microcomputer to be used as the data acquisition and analysis mechanism for this project. The program performs data acquisition, instrument control, data processing, file manipulation, and graphic outputting of results. [Ref. 19: p. 1-2] The subroutines in Acqwile are all menu driven and contain options for automatic probe calibration, plotting of calibration data with error analysis, data acquisition, vector conversion to reference coordinate system, and data storage.

Data analysis includes computation of mean, root mean square (RMS), turbulence intensities, skewness, flatness, and cross moments. It also performs calculation and display of the block averaged power spectral density for any channel, calculation and display of the single point autocorrelation function, and outputting graphic presentations to a plotter or printer. Unfortunately, this software was (and still is) in the process of development, contained many features that did not function properly, and it was the cause of many delays and much extra work.

#### IV. GENERAL SIMULATION

Developing an accurate simulation for the interface has been a feat that has not been accomplished with much confidence. Modeling the free stream airflow to the ship must be achieved with reasonable accuracy. Past efforts, such as White and Chaddock in 1967 [Ref. 24], used uniform velocity, very low turbulence, distributions in an attempt to simulate the real flow using a model of USS Lexington. Analysis by Loezos in that same year found that turbulence intensities were up to three times greater in the real environment than were recorded in the tunnel. [Ref. 25] Some ten years later, Boeing Vertol repeated the same mistake. [Ref. 3]

In Fortenbaugh's attempt at the complete interface simulation, he defined a data-base involving nine parameters. [Ref. 4: p. 2] They were:

- (1) Wind over deck magnitude -  $V_{WOD}$
- (2) Wind over deck direction relative to the ship -  $\psi_{WOD}$
- (3) Ambient wind magnitude -  $V_{WIND}$
- (4) Ship speed -  $V_s$
- (5) Ship's head relative to predominant wave direction  $\mu_s$
- (6) Ambient wind direction relative to ship -  $\psi_{WIND}$
- (7) Significant wave height -  $H_s$
- (8) Modal wave period -  $T_o$
- (9) Sea state - SS

The present project is concerned only with the resultant,  $V_{WOD}$  and the subsequent ship airwake along the approach path. The term "wind over deck" (WOD) is ambiguous and will not be

used here; the correct term, "relative" will be used instead. Future studies will attempt to model the ship's motion (oscillation) as a function of sea state, wave period, and significant wave height. Ship speed and true wind speed are not separated in the present study, since the ship is stationary. The relative velocity is then composed of the wind component only; this leads to the highest turbulence intensities and the worst-case scenario. A ship velocity component added to a given true wind will give an increased relative speed, and since the free-stream fluctuations will remain the same, the resultant turbulence intensity is reduced.

Fortenbaugh's airwake model is derived from the airwake data base established by Garnett in 1976 for the FF-1052. By using Strouhal number scaling, he assumed that the DD-963 and FF-1052 superstructures were similar enough that their Strouhal numbers would be the same. [Ref. 4: p. 7] Another important assumption for the airwake model is that airwake velocity components act on the aircraft center-of-gravity. For this project, using single point data, there is no choice but to accept this assumption. Future studies will consider the effects of non-uniform winds and turbulence on various components of the helo during approach, launch, and recovery. Moreover, in Fortenbaugh's model, full scale turbulence is represented as the product of the standard deviations of the

global airwake statistics and the first-order-lag-filtered white noise [Ref. 4: p. 9]. This replaces a second-order-lag-filtered system previously established [Ref. 26: p. 6]. Fortenbaugh took Garnett's data base, which was constructed as described in the Introduction and extracted, presumably by interpolation, the velocities, turbulence intensities and spectrum functions along two flight paths to the touch-down point. One path was along the ship longitudinal axis and the other at a 30° angle to starboard of the ship's axis; both paths approaching from the stern of the ship. A brief comparison will be made, in Chapter VI, between the present results and those presented there.

A more refined version of the turbulence model was presented by R.L. Nave also in 1978, using the same data base [Ref. 27: p. 2]. It is claimed that the first-order system reduced the degree of complexity, and increased the accuracy of the predictions. Hanson claimed an improvement on this model using a scheme involving linear interpolation to filter the output of the white noise; thus, the frequency content of the turbulence was regulated by varying the interval at which random number generators were called [Ref. 28: p. 2]. The result of this is that the high frequency content of the input signals is reduced prior to reaching the first-order-lag-filters. The white-noise is then shaped by the filters to simulate the effect of the environment on the helo and the

independent outputs from the x-, y- and z-direction simulations are fed to each of three servo-mechanisms that drive the simulator cab.

Hanson did not compare the predictions of his refined model with the experimental data base, but did attempt a validation of it using experienced pilots. The results indicated that reductions of 60-70% in the variances were required before the performance became somewhat realistic. [Ref. 28: p.31] It is clear that the single-point model needs much more study before it is considered viable or before it is abandoned in favor of a multi-point model.

The single-point data-base obtained in the present study will be used to replace the existing faulty one; validation of the interface will then be attempted using Hanson's improved filtering techniques.

The simulation of the influence of shear on a helo have been explored in several papers. (Clement and Jewell, 1985, [Ref. 29], Johns, 1986, [Ref. 30], and previously mentioned, Hansen, 1986, [Ref.28]) Evaluation of the Flying Qualities Requirements (FQRs) has also been made by John Johns using the NASA Ames Research Center's Vertical Motion Simulator, several Navy helo pilots, and a generic mathematical model of a single rotor helo known as "ARMCOP" [Ref. 30]. Quantification of the pilots' opinion was achieved using the Cooper-Harper Pilot Opinion Rating (CHPOR) which is an objective scale from "one"

(easily controllable) to "ten" (uncontrollable). Some of the simulation results did not clearly define boundaries for FQRs but they did shed some insight on the use of simulators in conducting flying quality tests. The overall pilot opinion was that the simulation was more difficult to fly than the real world helo. The primary reason for this is that the visuals for the VMS generate only crude, two-dimensional images which made it difficult for the pilots to realize depth perception. A major encouraging result of this test was that CHPOR ratings were fairly consistent among the pilots and naturally the pilots found it more difficult to "fly" the simulation with rougher sea states and wind conditions.

## V. EXPERIMENTAL PROCEDURE

The first step in this study was to calibrate the anemometer and the tunnel. Wind tunnel velocity and turbulence maps were drawn to establish reasonable uniformity of the flow and conformity to the required simulated boundary layer. This was followed by acquisition of a data-set for a "flight" through the clean tunnel along the desired flight path, which was always at an angle of  $4^{\circ}$  to the horizontal. Later runs, with the model in position, showed its influence on the boundary layer flow.

The reference frame for data acquisition was oriented so that "X" pointed in the direction of the flow, and had the component of the velocity of  $U$ , the "Y" component is the transverse (cross-tunnel) one, pointing to port, with the velocity component of  $V$  and the "Z" axis is vertical, and with the velocity component of  $W$ . This is a left-handed coordinate system and was chosen so that it was in compliance with the probe orientation.

For all flight-path runs the probe was 25 mm (1") above the touchdown point at the end of each "flight". Data were taken at 15 points of the following fractions of the ship length, aft of the touchdown point in the wake: 0 (at touchdown), 0.042, 0.084, 0.125, 0.139, 0.188, 0.253, 0.335,

0.418, 0.489, 0.565, 0.627, 0.732, 0.836, and 1.0. For reference, the length of the DD-963 is 171.6 meters (563 ft).

Three flight-paths to the flight-deck from the stern were considered: the 30° port, the stern (0°), and the 30° starboard approaches.

Data for the spectra were obtained from 16384 samples, which were acquired at 2.5 KHz and averaged over 32 blocks. No windowing was used and the analog low-pass filters were set at 3 KHz to reduce noise and aliasing. For the velocities, turbulence intensities, velocity histograms and auto-correlations, sample sizes of 8192 were used with a sampling frequency of 1 KHz. Finally, all data were processed and graphs drawn.

Preliminary runs showed extremely large levels - up to several hundred percent - of turbulence intensity for the transverse V, and vertical W, velocity components in the wake. These high values were a consequence of extremely small mean velocity values for these two components. When the Root Mean Square's (Rms) of the velocity fluctuations are made non-dimensional with the freestream velocity,  $U_a$ , at ship anemometer height, instead of the mean of V and W, the values are, in magnitude, comparable with those of the U component. Furthermore, these ratios are desirable data, since they are used in the simulation. All the velocities in the wake are made non-dimensional with  $U_a$ , for the latter reason.

## VI. DISCUSSION AND RESULTS

### A. CLEAN TUNNEL (NO MODEL PRESENT)

A mean velocity and turbulence intensity map for the clean (empty) tunnel was initially constructed as shown in Figure 15 from the data points of Table III. Fifty-six points (8 X 7 matrix) were taken in all for the map. The velocities show a reasonable uniformity across the test section (in the Y direction) and the turbulence intensity profiles are in the range given in Reference 2 for rough sea.

The mean velocity profile (of the mean U velocity) across the test section was found by a least squares fit to the data of Table III to have an index,  $n$ , of 0.135 - somewhat high for rough sea. The auto-correlation of the along-wind component at the elevations 50, 75, 100 and 200 mm (2", 3", 4" and 8") on the tunnel center-line in the clean tunnel are shown in Figure 16. The 75 and 200 mm levels are the elevations of the flight deck and ship anemometer respectively. The auto-correlations have the exponential-decay characteristic up to a characteristic time, which was estimated by the point where the ordinate had dropped to  $1/e = 0.368$  of its maximum. This characteristic time, when multiplied by the freestream velocity at this point, gives an estimate of the integral length scale. The values thus obtained were found to be 50,

Table III. Velocity and Turbulence Data as Functions of Position

VELOCITIES (m/s)

		Z - Height Above the Floor (mm)							
		50	75	100	125	150	200	500	810
% Tun. Width									
25.0		1.42	1.52	1.67	1.71	1.72	1.77	1.85	1.96
33.3		1.40	1.51	1.63	1.70	1.70	1.75	1.80	1.93
41.7		1.23	1.34	1.45	1.52	1.57	1.64	1.82	2.05
50.0		1.44	1.55	1.61	1.66	1.70	1.75	1.84	2.05
58.3		1.25	1.37	1.55	1.54	1.57	1.68	1.81	2.02
66.7		1.36	1.51	1.57	1.64	1.65	1.73	1.85	2.02
75.0		1.27	1.44	1.59	1.68	1.71	1.78	1.88	1.98
Mean		1.34	1.46	1.58	1.64	1.66	1.73	1.84	2.00
$\sigma$		0.09	0.08	0.07	0.08	0.07	0.05	0.03	0.05
$U/U_*$		0.61	0.66	0.71	0.74	0.75	0.78	0.83	0.91

TURBULENCE INTENSITIES (%)

		Z - Height Above the Floor (mm)							
		50	75	100	125	150	200	500	810
% Tun. Width									
25.0		15.5	12.7	8.8	7.6	6.6	6.4	6.5	4.2
33.3		14.8	11.2	8.6	7.7	7.4	6.8	6.3	4.5
41.7		16.4	12.9	10.9	9.3	9.2	8.2	5.4	3.6
50.0		12.8	10.2	8.8	7.5	7.4	6.7	5.2	2.9
58.3		16.0	13.2	10.5	9.5	9.0	7.6	5.9	3.2
66.7		13.0	9.8	8.4	7.2	6.8	6.5	6.2	3.2
75.0		16.8	12.8	10.2	8.1	7.4	5.8	4.8	3.7
Mean		15.0	11.8	9.4	8.1	7.7	6.8	5.8	3.6

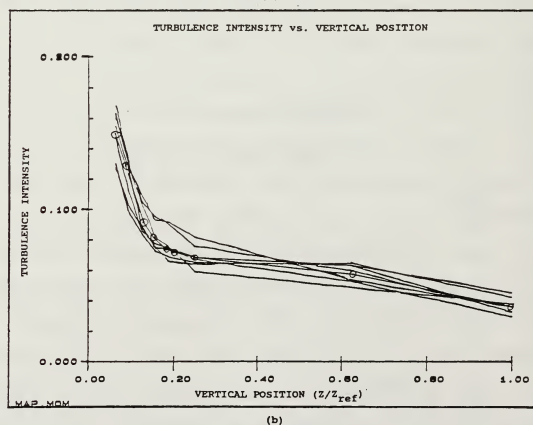
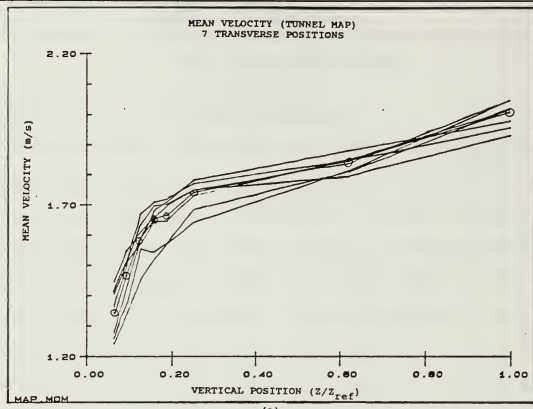


Figure 15. Velocities (a) and Turbulence (b) as Functions of Vertical Position of Boundary Layer

63, 80, and 44 mm respectively for the given elevations. The value at 200 mm seems to be an anomaly - possibly due to deviation from the exponential decay curve. There was insufficient time to do an integration to find the area under the curve, which would have given a more accurate estimate.

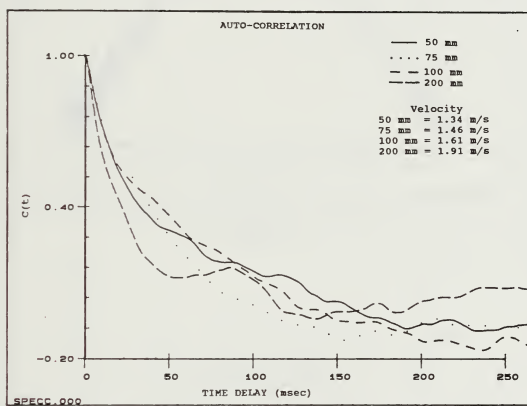


Figure 16. Autocorrelations of 50, 75 100, and 200 mm Vertical Position in Clean Tunnel

The spectrum functions for the  $u$  velocity component are shown in Figures 17 and 18. All exhibit the classic inertial sub-layer characteristics at high frequency, and peak at

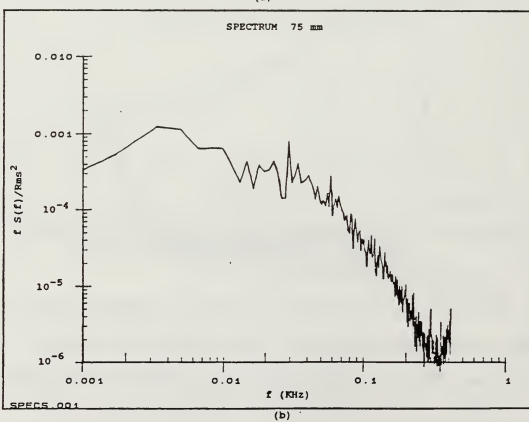
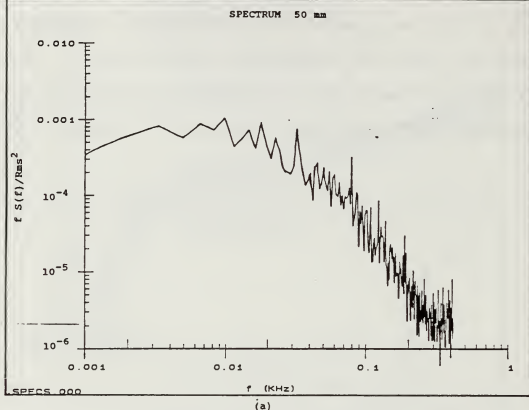
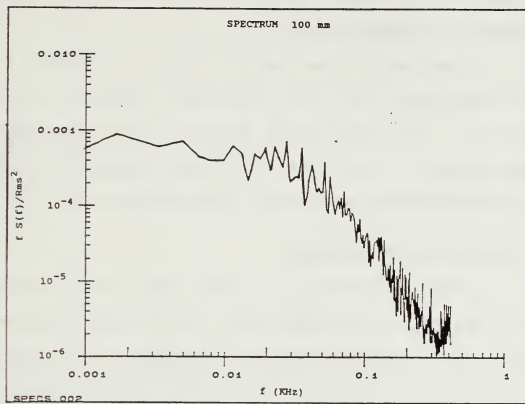
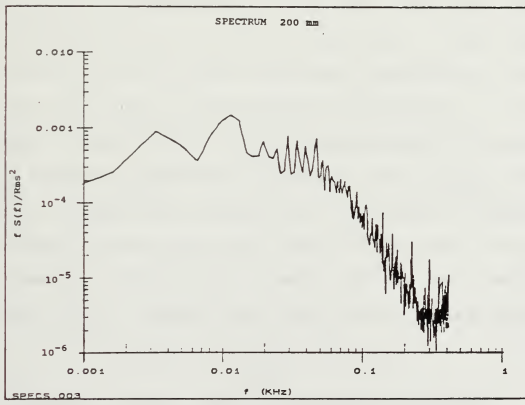


Figure 17. Spectrum Functions for (a) 50 mm and (b) 75 mm



(a)



(b)

Figure 18. Spectrum Functions for (a) 100 and (b) 200 mm

frequencies between 2 and 10 Hz. They were similar to atmospheric spectra. [Ref. 2]

The mean velocities and the turbulence levels, both made non-dimensional with the freestream velocity at anemometer height  $U_a$ , along the flight paths for the clean tunnel, are superimposed on the values for the corresponding flight path, and will be discussed in the next two sections.

#### **B. THE ZERO-YAW APPROACH**

The mean velocities  $U$ ,  $V$ , and  $W$ , made non-dimensional with  $U_a$ , along the stern flight path (at zero yaw relative to the ship axis), together with the profiles in the clean tunnel along the same flight path, are shown in Figures 19 and 20. The clean-tunnel value of  $U$  never drops below 0.9  $U_a$  but, with the model,  $U$  drops down to about 0.18 of  $U_a$  over the flight deck and gradually recovers to about 0.8 of  $U_a$  one ship-length away. The deviation of the mean of  $V$  from the clean-tunnel value is less than about 10% of  $U_a$  and gradually approaches it with distance from the ship. The  $W$ -component shows a somewhat anomalous behavior. The values with and without the model are almost identical and both values are slightly negative. Some unevenness in the tunnel floor giving a small ( $2.5^\circ$ ) misalignment of the probe could account for this behavior.

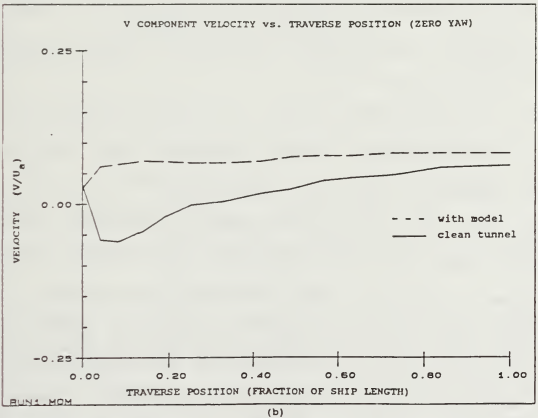
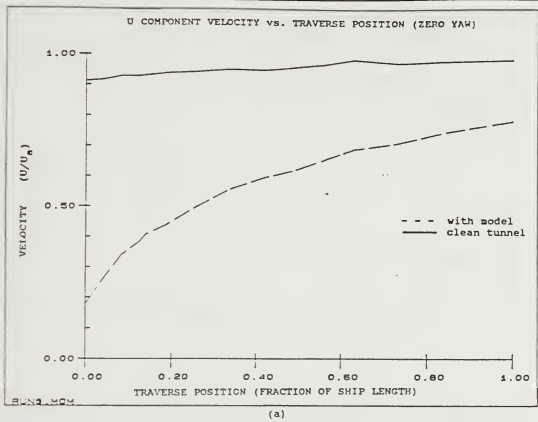


Figure 19. U (a) and V (b) Component Velocities vs. Traverse Position

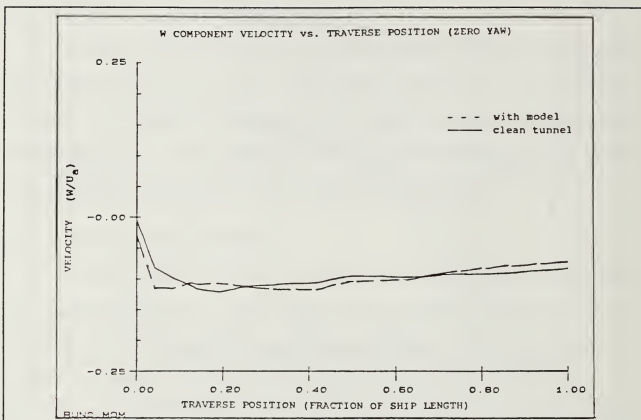


Figure 20. W Component Velocity vs. Traverse Position

The along-wind turbulence intensity is plotted in Figure 21. The lower curve is for the clean tunnel and shows the value dropping from about 12% to about 7%. With the model, there is a rapid increase of intensity from about 29% to about 35% in about 5% of a shiplength, followed by a very rapid decline to about 14%. The other turbulence values, given by the RMS values for U, V, and W divided by  $U_a$ , appear in Figure 22; these show the U and W profiles growing rapidly to about 10% and the V-profile more slowly to about 8%. Figures 23 and 24 are histograms of the U-component of velocity and

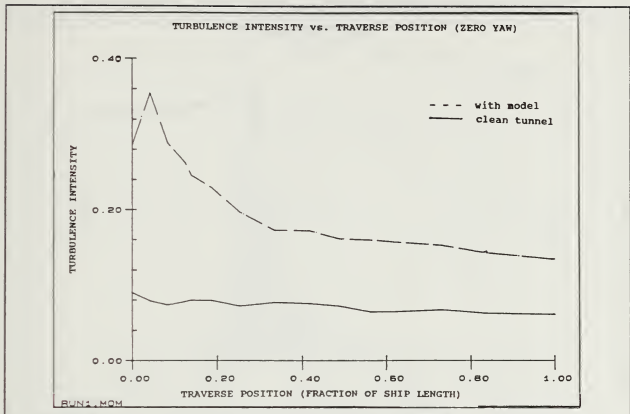


Figure 21. Turbulence Intensity vs. Traverse Position

show a distribution that is very skewed from the Gaussian for the flight deck point, 23(a) and the next point aft, 23(b). This throws suspicion on the turbulence measurements at these two points. Further aft, there is a rapid recovery to the Gaussian distribution with distance from the ship. Full recovery is seen at about 1/4 ship length aft of the touchdown point.

The auto-correlation over the flight deck yields an estimate showing that the along-wind length scale has been reduced by a factor of four, relative to the value in the clean tunnel. This scale, however, gradually approaches the

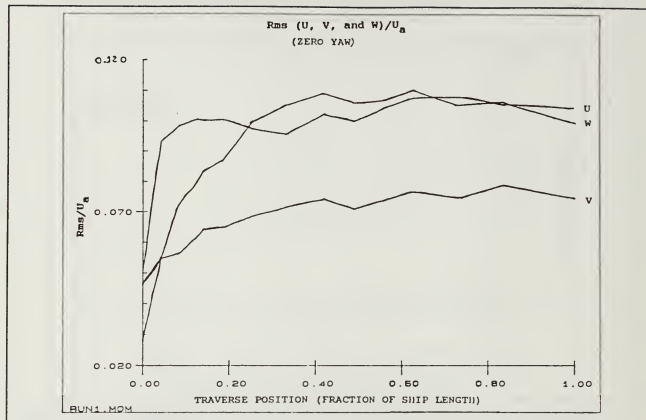


Figure 22.  $Rms/U_a$  vs. Traverse Position

clean-tunnel value with distance from the ship and equals it at one ship length. These auto-correlations are shown in Figures 25 and 26.

The Spectrum functions are depicted by Figures 27 and 28. There is a noticeable flattening of all these spectra relative to the ones described in Section A above; it appears that the presence of the model reduces substantially the low frequency energy in the flow, resulting in flatter spectra. Energy distributions above about 100 Hz are not affected.

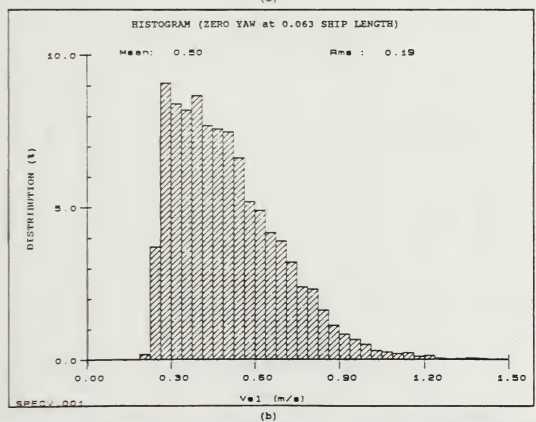
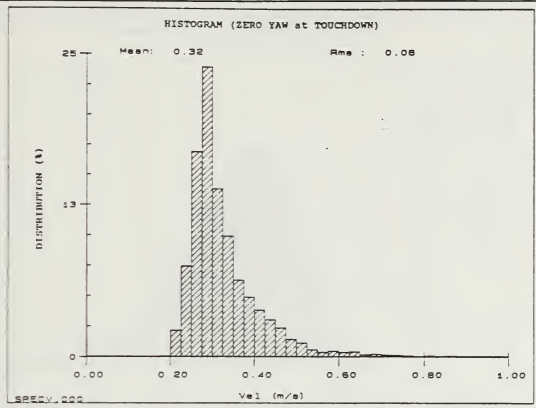


Figure 23. Velocity Histograms at (a) Touchdown and (b) 0.063 Ship Length (Zero Yaw)

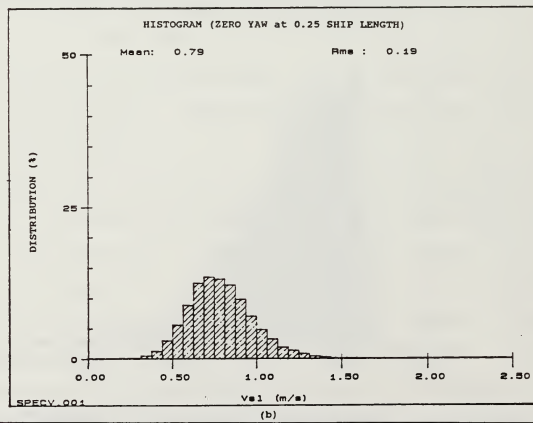
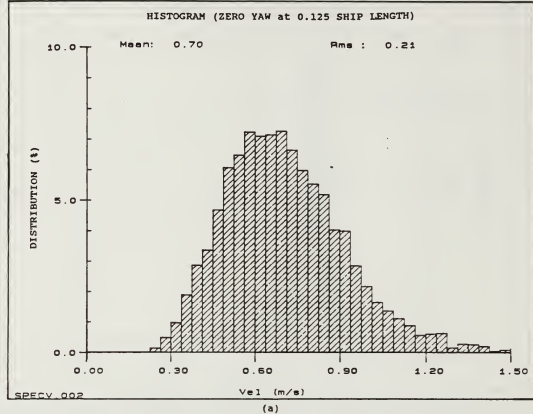


Figure 24. Velocity Histograms at (a) 0.125 and (b) 0.25 Ship Length (Zero Yaw)

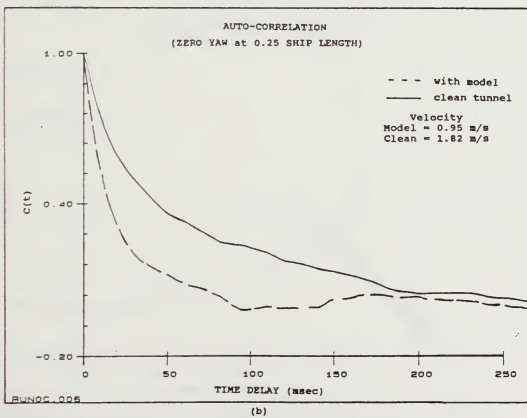
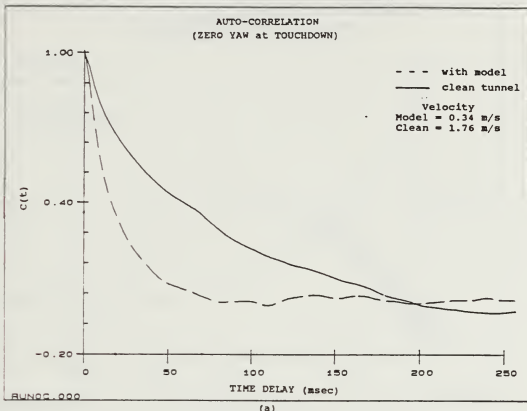


Figure 25. Auto-Correlations at (a) Touchdown and  
(b) 0.25 Ship Length (Zero Yaw)

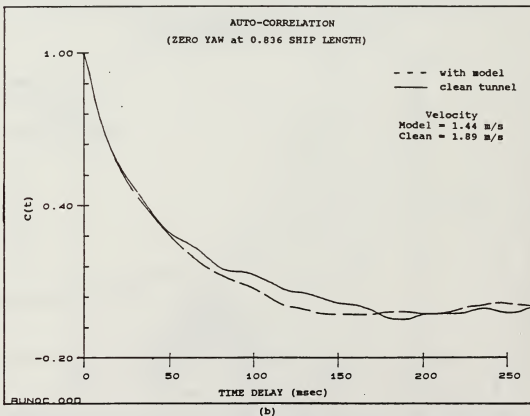
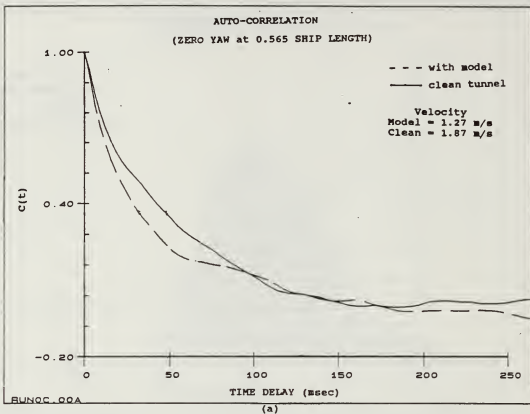


Figure 26. Auto-Correlations at (a) 0.565 and (b) 0.836 Ship Lengths (Zero Yaw)

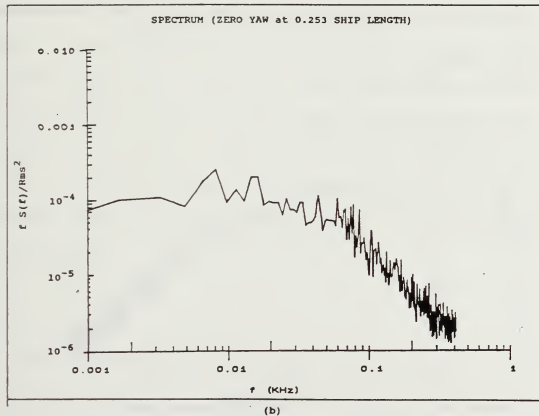
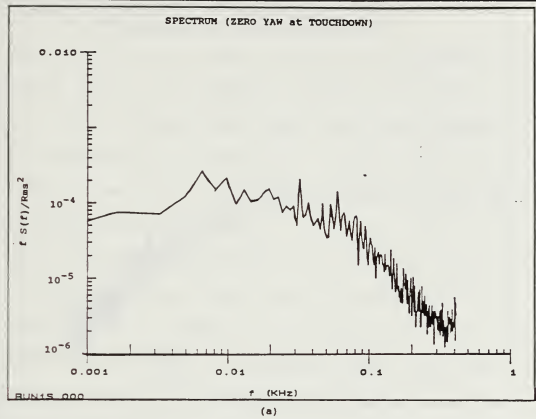


Figure 27. Spectrum at (a) Touchdown and  
(b) 0.253 Ship Length (Zero Yaw)

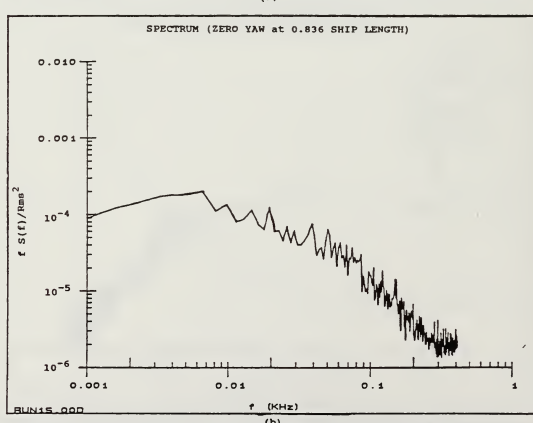
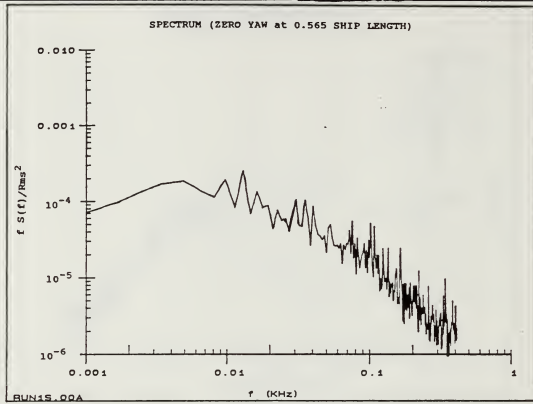


Figure 28. Spectrum at (a) 0.565 and  
(b) 0.836 Ship Lengths (Zero Yaw)

### C. $30^\circ$ Port and Starboard Yaw Approaches

Due to the fact that the model was moved to the yaw positions about its geometric center (vice helo touchdown point), both  $30^\circ$  approaches had their own respective clean tunnel approach data runs taken. This section will compare the two with each other and make reference to the  $0^\circ$  yaw data in the previous section.

The individual components of the mean velocities were plotted against clean tunnel runs and are shown in Figures 29, 30, and 31. The U component velocities are nearly identical for all three (port, starboard, and  $0^\circ$ ) runs however variations in the V and W components can be seen. Moving aft along the flight path, the V component appears to move away from the clean tunnel value for the port approach where the starboard approach V component moves eventually moves toward the clean tunnel value. In any case the magnitudes are still less than 10% of  $U_a$ . Both W components increase rapidly within a 20% ship length and show a peak at about 10%  $U_a$ . Moreover, both stay within about 15% of one another along the approach path.

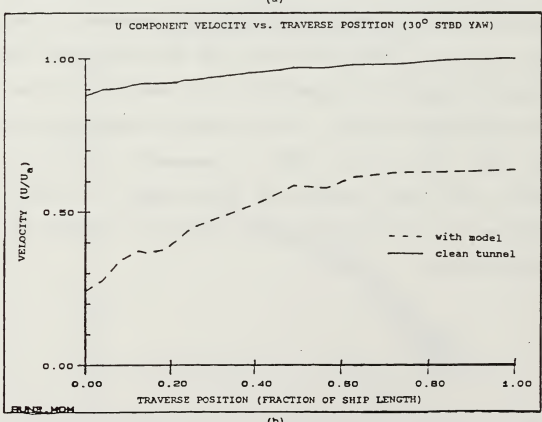
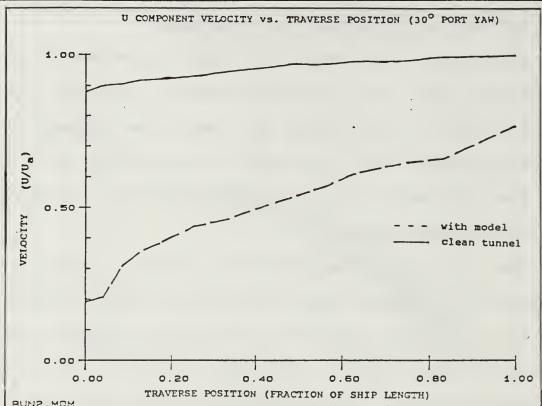
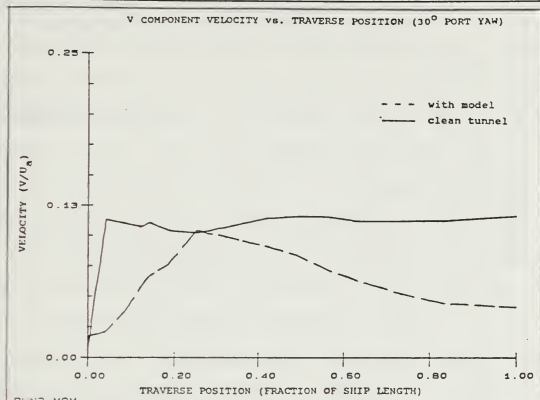
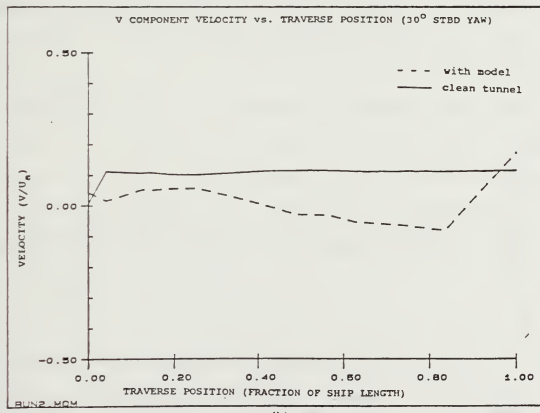


Figure 29. U Component Velocities vs. Traverse Position  
 (a)  $30^\circ$  Port and (b)  $30^\circ$  Stbd Yaw



(a)



(b)

Figure 30. V Component Velocities vs. Traverse Position  
 (a)  $30^{\circ}$  Port and (b)  $30^{\circ}$  Stbd Yaw

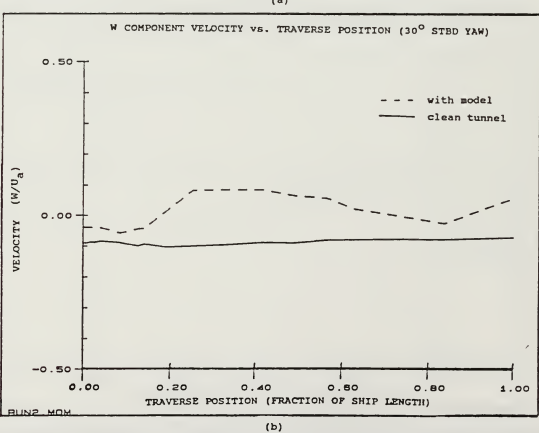
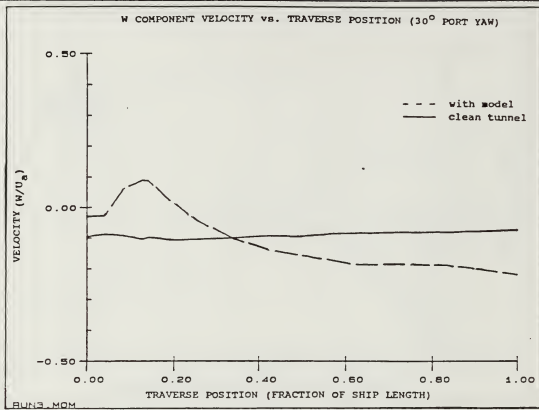


Figure 31. W Component Velocities vs. Traverse Position  
 (a) 30° Port and (b) 30° Stbd Yaw

Turbulence intensities for both  $30^\circ$  runs are similar in shape to those of the  $0^\circ$  data with the exception that the starboard run magnitude is greatest, peaking above 50% at the touchdown point. The port approach peak has also a large turbulence level of 46% just aft of the touchdown point. Both graphs of turbulence are shown in Figure 32. As with the  $0^\circ$  yaw run, the histograms for the U components of velocity are skewed drastically at the touchdown point and recover rapidly to an approximately Gaussian shape distribution by  $1/4$  ship length aft of the touchdown point. Figures 33 and 34 show the histograms at the touchdown and the 6% aft points respectively. Once again, turbulence levels at these points are suspect, as was noted in Section B for the  $0^\circ$  run. Rms values for U, V, and W divided by  $U_a$  (Figure 35) show that, like the  $0^\circ$  run, U and W components increase more rapidly and are higher in magnitude (to about 15%) than the V component which levels at 8%. This measure of turbulence agrees with the previous measure of turbulence intensity in that turbulence for the  $30^\circ$  runs are about 5% greater than that found in the  $0^\circ$  run.

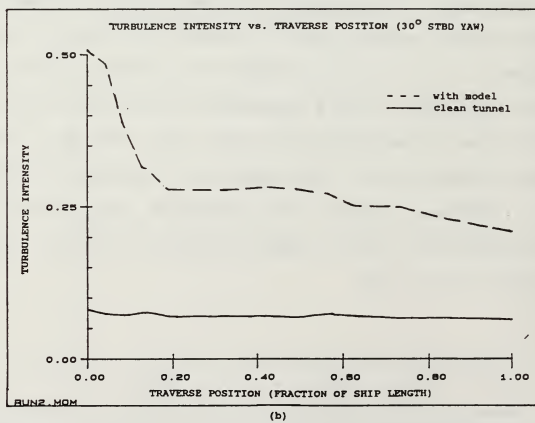
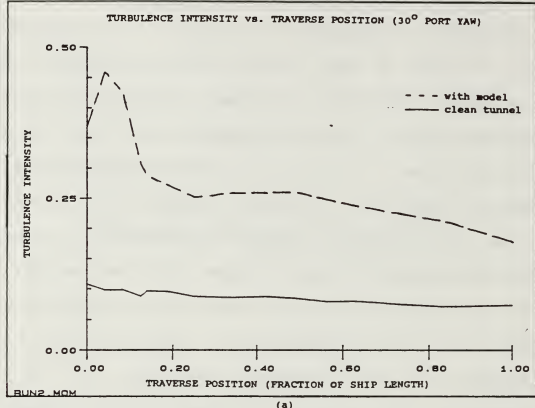


Figure 32. Turbulence Intensities vs. Traverse Position  
 (a)  $30^\circ$  Port and (b)  $30^\circ$  Stbd Yaw

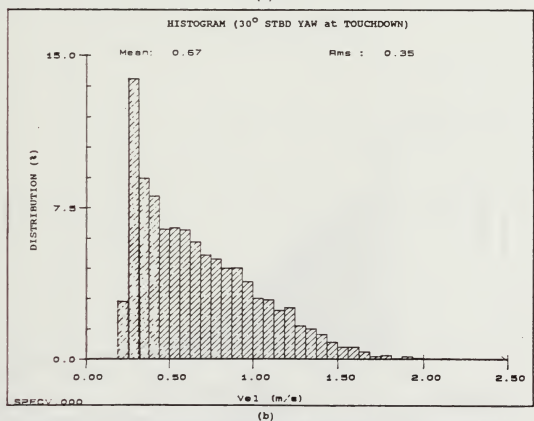
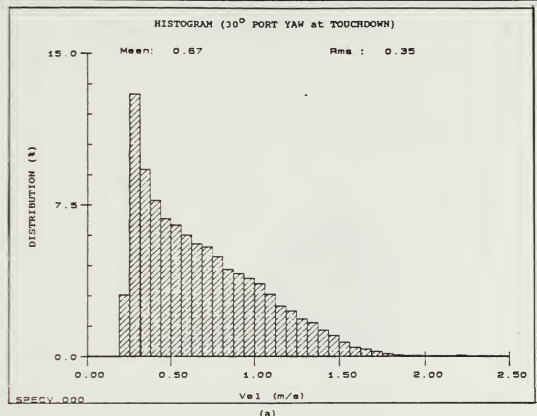


Figure 33. Velocity Histograms (a) 30° Port and (b) 30° Stbd Yaw at Touchdown

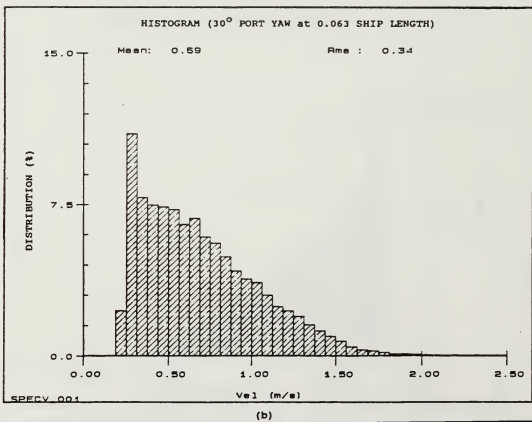
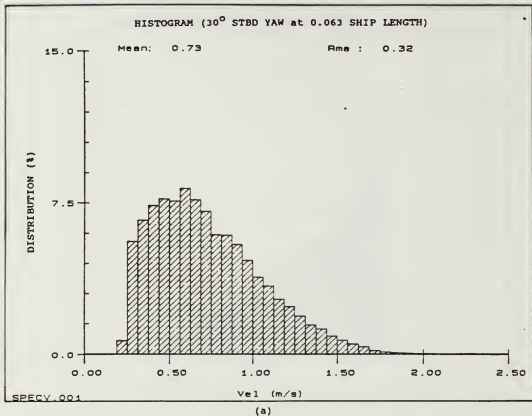


Figure 34. Velocity Histograms at (a)  $30^\circ$  Port and (b)  $30^\circ$  Stbd Yaw at 0.063 Ship Length

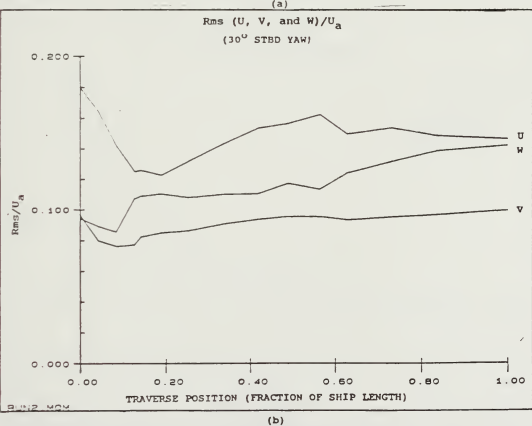
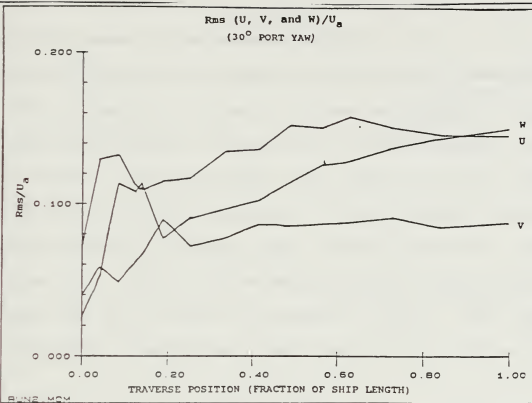


Figure 35. Rms/U<sub>a</sub> vs. Traverse Position for  
(a) 30° Port and (b) 30° Stbd Yaw

The analysis of the auto-correlation shows that there is consistency with all three tunnel runs in that the along-wind length scale is reduced by a factor of sixteen at the flight deck touchdown point in reference to those values found in the clean tunnel and that full scale recovery is found at about one ship length from the touchdown. The auto-correlations are shown in Figures 36-39. The starboard approach graphs show an oscillation at lag times beyond 50 msec not seen in the port runs; however, at the 36.8% point used for determining the length scales, the graphs are virtually identical.

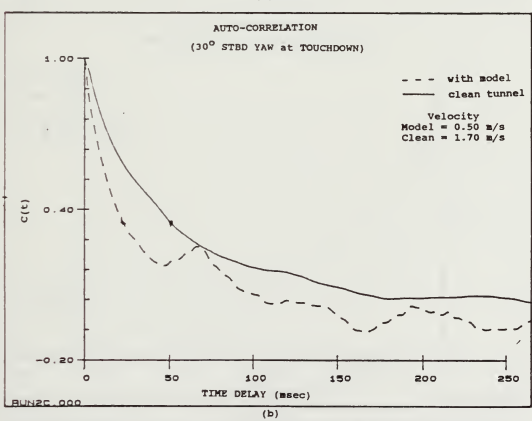
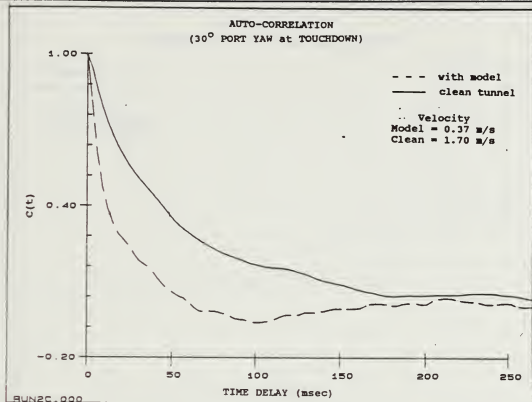


Figure 36. Auto-Correlations (a) 30° Port and  
(b) 30° Stbd at Touchdown

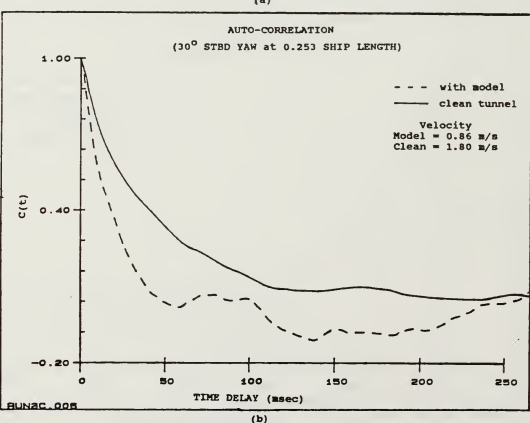
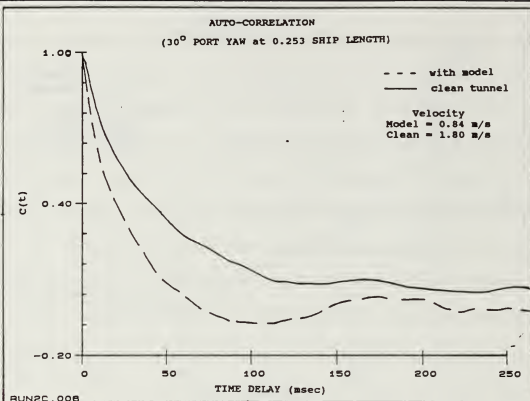
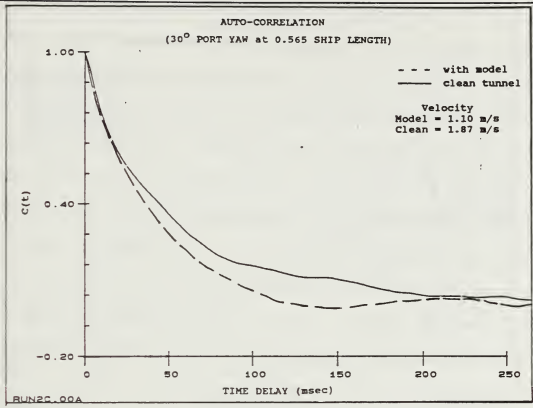
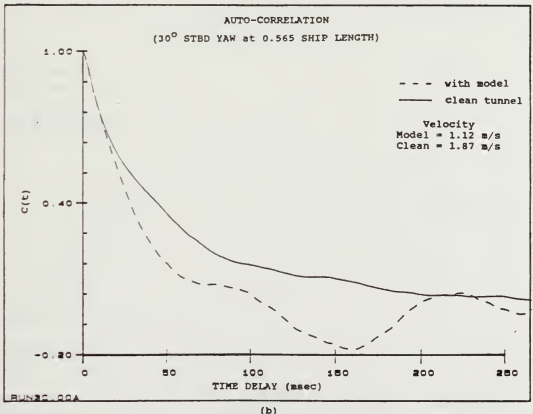


Figure 37. Auto-Correlations (a) 30° Port and  
(b) 30° Stbd at 0.253 Ship Length



(a)



(b)

Figure 38. Auto-Correlations (a) 30° Port and  
(b) 30° Stbd Yaw at 0.565 Ship Length

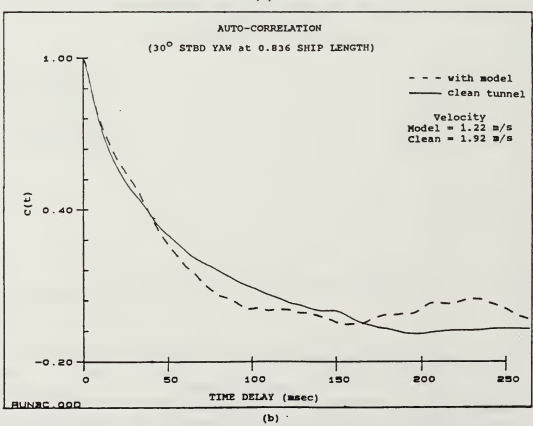
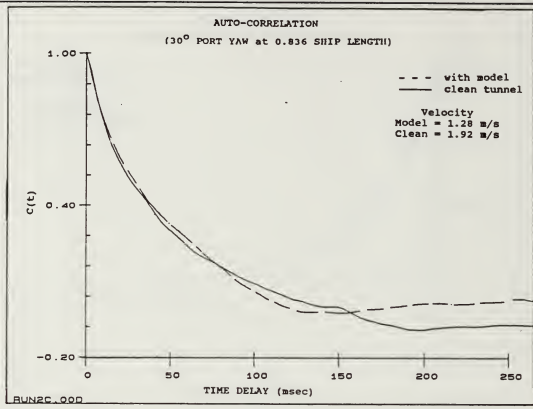


Figure 39. Auto-Correlations (a) 30° Port and  
(b) 30° Stbd Yaw at 0.836 Ship Length

The Spectrum functions (Figures 40-43) show the same general flattening as observed in the 0° run and it can be observed that the starboard yaw contains more energy than that of the port runs and, referring to Figures 27 and 28, more energy than that of the 0° runs. This can be attributed to the higher levels of turbulence in the starboard approach.

At the flight deck, neither the starboard nor the port runs show significant peaks in the spectrum function below 10 Hz as was observed in the 0° run. As the approach path is traversed, specific frequency peaks can be seen between 3 and 30 Hz.

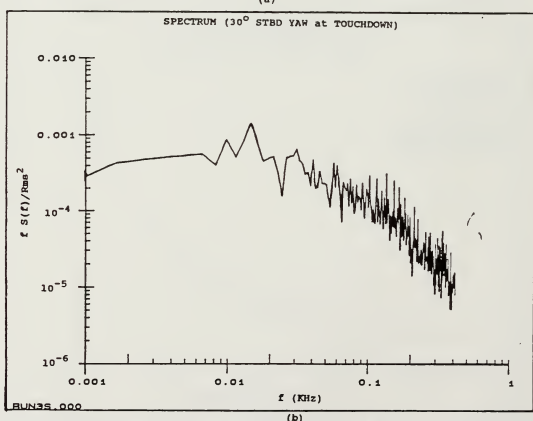
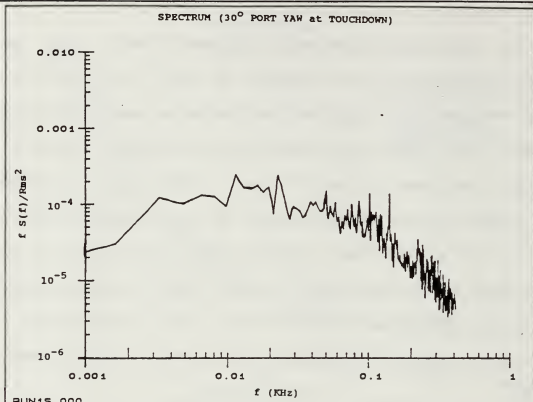


Figure 40. Spectrum (a) 30° Port and (b) 30° Stbd Yaw at Touchdown

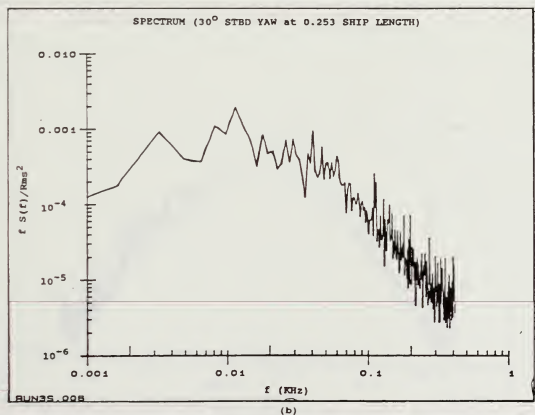
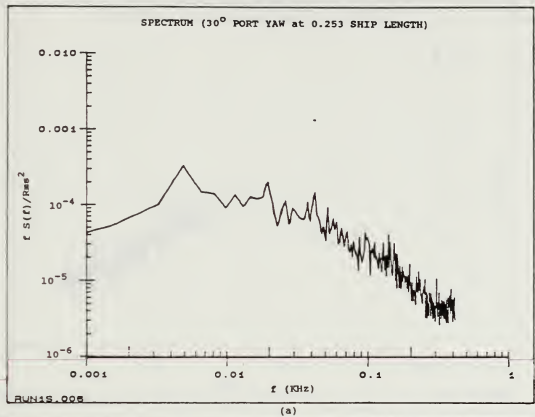


Figure 41. Spectrum (a)  $30^\circ$  Port and (b)  $30^\circ$  Stbd Yaw at 0.253 Ship Length

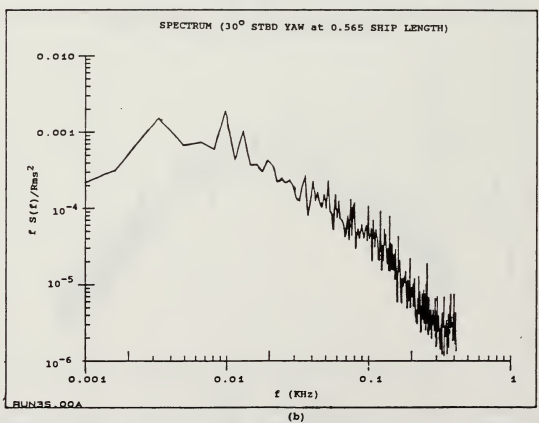
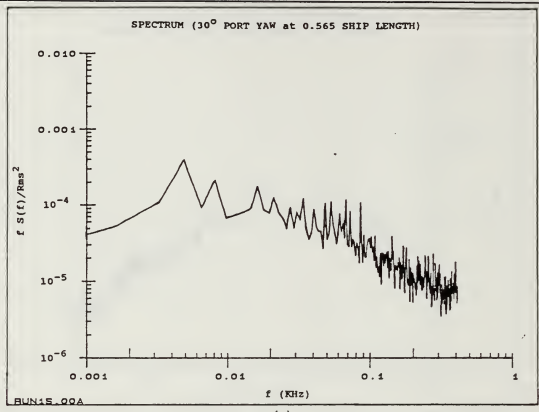
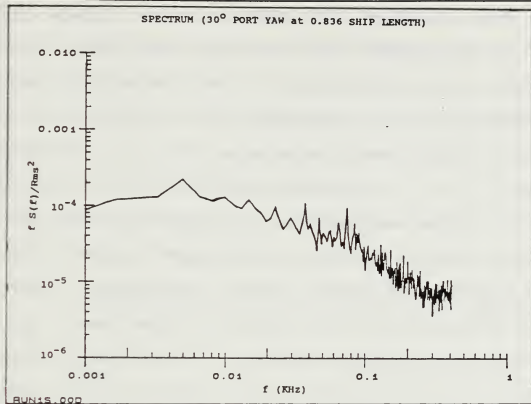
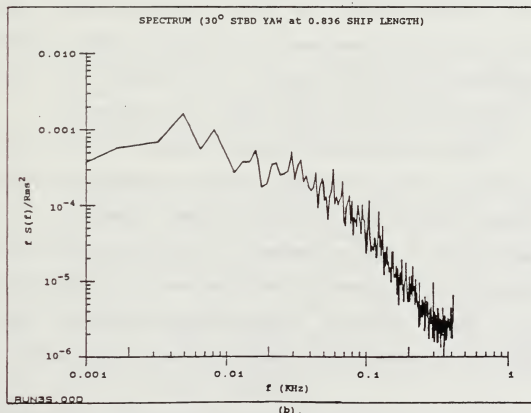


Figure 42. Spectrum (a)  $30^\circ$  Port and (b)  $30^\circ$  Stbd Yaw at 0.565 Ship Length



(a)



(b)

Figure 43. Spectrum (a)  $30^\circ$  Port and (b)  $30^\circ$  Stbd Yaw at 0.835 Ship Length

#### **D. BRIEF COMPARISON WITH PREVIOUS DD-963 AIRWAKE STUDY**

Recalling that since the major difference between the tests run by Garnett [Ref. 5], the mathematical analysis of Fortenbaugh [Refs. 4 and 26], and this project is that the velocity profiles and turbulence levels were different (See Figure 1), it is reasonable that the results of this project would yield higher levels of turbulence and lower velocities. In fact, this is the case. Fortenbaugh's analysis showed that the component velocities' standard deviations, divided by the free stream velocity at anemometer height (Rms/U bar), as a measure of turbulence, reduces to near zero at one ship length from the touchdown point for all three velocity components. [Ref. 26: pp. 63-65] The results of this project show that this is not the case and the effects of the environmental atmospheric velocity profile are obvious with turbulence intensity levels of 15-25% evident at this point.

A similarity in the two sets of results is that turbulence intensity levels are significantly reduced (40-50% for this project, 50-75% for the Boeing data) within 25% of a ship length aft of the touchdown. In general, differences of several factors in both velocities and turbulence intensities were found. Only in a qualitative sense was there much agreement between these results and the Boeing data.

## VII. CONCLUSIONS AND RECOMMENDATIONS

The results of this study indicate that a plausible airwake data base for the DD-963 has been established. Its efficacy must ultimately be established by its successful integration into a suitable simulator.

Some recommendations for future studies are:

- (1) Test of these data in the NASA simulator.
- (2) Investigate the wake using larger models in an expanded test section to obtain better measurement resolution.
- (3) Study the influence of ship oscillations on the wake.
- (4) Examine the influence of scale on the data and on the relative success of the simulation.
- (5) Since the project concerned itself with a helo flying directly into a ship's relative wind (which is not always the case in the real world), expanded studies should accompany the present project to include, (in addition to those mentioned in the Introduction) helos approaching at angles other than that of straight into ship's relative wind.
- (6) Obtain a better software program for data acquisition and analysis. The present software package "Acqwir" is still under development and, as was mentioned previously, was the cause of numerous delays in this project. Malfunctions of the program include: (but are by no means limited to) the inability to apply windowing to spectrum functions even though the capability is (supposedly) there, the inability to scale graphs and plot them without causing the entire computer system to "lock-up," and failure to include an accurate operating manual with the numerous changes that have been received.
- (7) Use electronic linearizers for all three channels and check the higher turbulence intensity values.

#### LIST OF REFERENCES

1. Johns, M. K., *Flow visualization of the Airwake Around a Model of a DD-963 Class Destroyer in a Simulated Atmospheric Boundary Layer*, M.S. Thesis, Naval Postgraduate School, Monterey, California, September 1988.
2. Healey, J. Val., *Simulating the Helicopter/Ship Interface as an Alternative to Current Methods of Determining Safe Operating Envelopes*, Naval Postgraduate School Report, NPS 67-86-003, Monterey, California, September 1986.
3. Garnett, T. S. Jr., *Investigation to Study the Aerodynamic Ship Wake Turbulence Generated by an FF-1052 Frigate*, Boeing Vertol Report D210-11140-1, December 1976.
4. Fortenbaugh, R. L., *Progress in Mathematical Modelling of the Aircraft Operational Environment of DD-963 Class Ship*, AIAA Paper No. 79-1677, August 1979.
5. Garnett, T. S. Jr., *Investigation to Study the Aerodynamic Ship Wake Turbulence Generated by a DD-963 Destroyer*, Boeing Vertol Report D210-11545-1, August 1979.
6. E.S.D.U. Data Items 74030, 74031, Engineering Sciences Data Unit International, Suite 200, Chain Bridge Road, McLean, Virginia, 22101.
7. Davenport, A. G., in *Engineering Meteorology*, E. J. Plate, Editor, Amsterdam, Netherlands, pp 527-569, Elsevier Scientific Publishing Company, 1982.
8. Plate, E. J., *Engineering Meteorology*, pp 573-636, Elsevier Scientific Publishing Company, 1982.
9. Bradshaw, P., *An Introduction to Turbulence and its Measurement*, Pergamon Press, Oxford, 1971.
10. Naval Air Engineering Center NAEC-ENG-7526 Rev AF, *Shipboard Aviation Facilities Resume*, Department of the Navy, Naval Air Engineering Center, Lakehurst, New Jersey, p.107, 1 April 1988.
11. Naval Warfare Publication (NWP-42 Rev. G), *Shipboard Helicopter Operating Procedures*, App B, Washington D.C., Department of the Navy, December 1986.

12. DISA Electronics (Dantec), *DISA Probe Manual*, Denmark, 1982.
13. Goldstein, R. J., *Fluid Mechanics Measurements*, Hemisphere Publishing Corporation, 1983.
14. Dantec Corporation, *56C17 CTA Bridge Instruction Manual*, Dantec Documentation Department, Denmark, undated.
15. Perry, A. E., *Hot-wire Anemometry*, Oxford University Press, 1982.
16. Blackwelder, R. F., *Methods of Experimental Physics: Fluid Dynamics*, R. J. Emrich, Editor, New York, pp 259-314, Academic Press, Inc., 1981.
17. Dantec Elektronic, *56N21 Linearizer Instruction Manual*, Dantec Documentation Department, Denmark, undated.
18. Dantec Elektronic, *Type 55D90 Calibration Equipment*, DISA Information Department, Denmark, undated.
19. Dantec Elektronic, *"acqWIRE" Technical Reference Manual*, Dantec Electronics, Inc., Allendale, N. J., 1989.
20. Digital Equipment Corporation, *Laboratory Instruction Manual*, Santa Clara, California, 1986.
21. MetraByte Corporation, *Dash 16/16F Manual*, Taunton, Mass., 1986.
22. Tri Sigma Corporation, *Model 8300 Series Software and Hardware Reference Manual*, Version 4.0, Tucson, Az., 1987.
23. Bolinger, W. K., *Visualization of the Flow Field Around a Generic Destroyer Model in a Simulated Turbulent Atmospheric Boundary Layer*, M.S. Thesis, Naval Postgraduate School, Monterey, California, June 1987.
24. White, H. E. and D. R. Chaddock, *Comparison of Full Scale and Model Data of the Wind Velocity over the CVS-16 Flight Deck*, DTNSRDC Report 2368, Aerodynamic Report 1128, April, 1967.
25. Loezos, S., *Effect of an Ambient Turbulence Component on Model Carrier Turbulence Data*, DTNSRDC Aerodynamics Lab. Report 1131, 1967.
26. Fortenbaugh, R. L., *A Math Model for the Airwake of a DE-1052 Class Ship*, Report No. 2-53300/7R-3397, Vought Corporation, 13 May 1977.

27. Nave, R. L., *Development and Analysis of a CVA and an FF-1052 Ship Airwake Model*, NADC-78182-60, 1978.
28. Hanson, G. D., *Airwake Analysis, Systems Technology, Inc.*, Working Paper No. 1198-3, September, 1983.
29. Clement, W. F. and W. F. Jewell, *Piloted Simulation Study of Helicopter Shipboard Landing to Determine Flying Qualities Requirements*, NADC-82151-60, November, 1985.
30. Johns, J., *Realtime Piloted Simulation Investigation of Helicopter Flying Qualities During Approach and Landing on Non-Aviation Ships*, Systems Technology, Inc. Paper, 1986.

**INITIAL DISTRIBUTION LIST**

	No. Copies
1. Defense Technical Information Center Cameron Station Alexandria, Virginia 22304-6145	2
2. Library, Code 0142 Naval Postgraduate School Monterey, California 93943-5000	2
3. Department Chairman, Code 67 Department of Aeronautics and Astronautics Naval Postgraduate School Monterey, California 93943-5000	1
4. Commander Naval Air Systems Command Air Vehicle Division Attn: Mr. Jonah Ottensoser, Code Air 53011C Jefferson Plaza 2, Rm. 904 Washington, D.C. 20361	2
5. Mr. Bernard Ferrier CANDAIR LTD. 1800 Laurentieu Blvd. Saint Laurent Quebec, Canada H4R1KZ	1
6. Naval Air Test Center Attn: Mr. Dean Carico, Code RW40A Patuxent River, Maryland 20670	1
7. Naval Air Test Center Attn: Mr. Jerry Higman, Code RW81 Patuxent River, Maryland 20670	1
8. Dr. J. Val Healey, Code 67He Department of Aeronautics and Astronautics Naval Postgraduate School Monterey, California 93943-5000	11

9. Mr. R.A. Feik 1  
Aeronautical Division  
Aeronautical Research Laboratories  
506 Lorimer Street  
Fisherman's Bend  
Box 4331 P.O.  
Melbourne, Victoria 3001  
Australia

10. Naval Air Test Center 1  
Code RW40, Attn: Kurt Long  
Patuxent River, Maryland 20670

11. Mr. Tony Cricelli, Code 67 1  
Department of Aeronautics and Astronautics  
Naval Postgraduate School  
Monterey, California 93943-5000

12. Lt. G.A. Anderson 1  
Surface Warfare Officer School  
Department Head Class 112  
Newport, Rhode Island 02841-5012

6/4-583









Thesis  
A4536      Anderson  
c.1              Mapping the airwake of  
                    a model DD-963 along  
                    specific helicopter  
                    flight paths.

Thesis  
A4536      Anderson  
c.1              Mapping the airwake of  
                    a model DD-963 along  
                    specific helicopter  
                    flight paths.



thesA4536

Mapping the airwake of a model DD-963 a/



3 2768 000 89087 5

DUDLEY KNOX LIBRARY